Higher-order beam model for stress predictions in curved beams made from anisotropic materials

C. Thurnherr[a,*], R.M.J. Groh[b], P. Ermanni[a], P.M. Weaver[b]

[a] *Laboratory of Composite Materials and Adaptive Structures, Department of Mechanical and Process Engineering, ETH Zürich, Tannenstr. 3, CH-8092 Zürich, Switzerland*

[b] *Advanced Composites Centre for Innovation and Science, University of Bristol, Queen's Building, University Walk, Bristol, BS8 1TR, UK*

Abstract

A higher-order beam model for analyzing the flexural response of curved multilayered beams with constant curvature and arbitrary constant thickness is developed. The new model is derived from the Hellinger-Reissner mixed variational statement and predicts inherently equilibrated 3D stresses from an equivalent single-layer model. As a starting assumption, the hoop stress is formulated as a series of higher-order stress resultants multiplied by Legendre polynomials. The governing equations are derived in a generalized manner such that the modeling order can be adjusted and is not defined a priori. Hence, the highest order Legendre polynomial determines the modeling order. The through-thickness shear and normal stresses are derived by integrating the generalized hoop stress in Cauchy's polar equilibrium equations. As a result, all stress fields are based on the same set of variables, thereby considerably reducing the computational effort. The three stress fields, and two displacements in the radial and hoop directions are used in the Hellinger-Reissner functional to derive a new set of stress-displacement relations. The enforcement of the classical membrane and bending equilibrium equations of curved beams in the Hellinger-Reissner functional guarantees that all interlaminar and surface traction equilibrium conditions are satisfied exactly. A validation study of a composite laminate using a high-fidelity 3D finite element model shows that the stresses are captured very accurately by the present model, but with much less computational effort than the finite element model. As a result, the developed model can provide rapid and accurate insights into the expected damage onset behavior of curved laminates.

Keywords: curved multilayered beams, higher-order modeling, interlaminar stresses, anisotropic materials

1. Introduction

Due to their lightweight structural properties, composite materials are increasingly used in primary aircraft structures. In areas of high curvature, as for example in T-shaped stringers of aircraft wings, interlaminar stresses are pronounced and can lead to premature delamination failure [1, 2]. To mitigate this debonding failure, it is crucial to robustly predict the stress fields in these curved laminated structures [3, 4, 5].

Recently, Most et al. [3] emphasized the importance of accurate stress prediction for delamination failure in thick curved composites. The researchers compared different models in the literature and concluded that finite element (FE) models are able to predict stress fields accurately, but with enormous computational costs, whereas models based on first-order shear theory are easy and fast to use, but are not capable of predicting stresses with high accuracy. Therefore, there is a need for new models that capture the higher-order structural effects that influence through-thickness shear and through-thickness normal stresses, but are economical in terms of computational resources.

Some models in the literature predict interlaminar stresses in curved beams based on the first-order shear deformation theory [6, 7]. These models typically derive a closed-form solution, which is economical in terms of computational cost, but do not take into account higher-order phenomena, and hence are only accurate for very thin laminates [8]. Kress et al. [9] derived a model to analyze radial stresses in moderately thick curved laminates. Roos et al. [10] improved this model by taking into account the interlaminar shear stresses. The model provides a closed-form solution, and hence does not need a lot of computational effort. However, in comparison with 3D FE, the model pre-

*Corresponding author

Email address: thclaudi@ethz.ch (C. Thurnherr)

dicts the stresses only to a certain accuracy. 3D FE can provide accurate stress fields predictions, but they are based on partial differential equations which are typically costly to solve [8]. Fraternali et al. [11] suggested an FE model based on the Principle of Virtual Displacements (PVD) where each layer is modeled as a beam element and individual layers are bonded together with a constraint enforced via a penalty method. Gonzalez-Cantero et al. [12] proposed a semi-analytical method to calculate interlaminar stresses in curved beams with constant curvature. Other authors conducted experiments to verify the real behavior of curved laminates [10, 13], but these tests cannot serve as a general strategy to predict delamination failure.

An example stress distribution in a curved beam is shown in figure 1. We expect an accurate model to be capable of predicting the hoop stress σ_φ considering higher-order effects such as stress channeling, i.e. a cubic rather than linear stress variation towards the top and bottom surfaces [14], as observed in figure 1. Further, the model needs to be able to recover the through-thickness stresses $\sigma_{r\varphi}$ and σ_r correctly, as these are crucial for the prediction of delamination failure. These transverse stresses need to fulfill the interlaminar stress continuity through the thickness and equilibria of tractions on the surfaces [15]. All these requirements are fulfilled in the model we present herein.

The objective of this paper is to present a new higher-order beam model for laminated curved beams. In section 2 the derivation of the governing equations is presented. First, the hoop stresses are expressed as a generalized Taylor series expansion of higher-order stress resultants multiplied by Legendre polynomials. The transverse stress fields are then derived by integrating the hoop stress in Cauchy's equilibrium equation written in polar coordinates. Next, the Hellinger-Reissner mixed variational statement is used to derive new higher-order stress-displacement relations that, alongside the classical membrane and bending equations of a curved beam, encompass the governing field equations of the theory. The use of this formulation is inspired by a model for flat composite beams presented by Groh and Weaver [16]. The end of section 2 details how the governing equations are solved using the pseudo-spectral differential quadrature method. The results of the new model are compared with a high fidelity 3D FE model in section 3. Further, the results are compared with closed-form first-order models by Timoshenko [17] and Kedward et al. [18]. A convergence study is presented to obtain the modeling order required to calculate accurate stress fields for the laminations and geometries studied herein. Finally, the accuracy of the stress fields com-

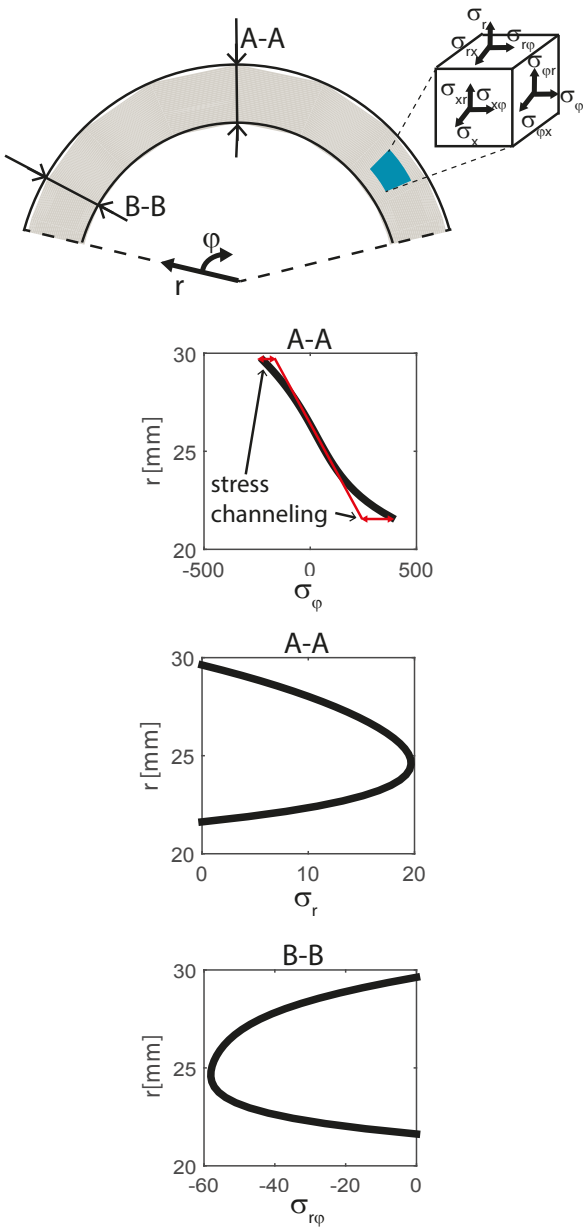

Figure 1: Illustration of stress distribution in curved beams. The hoop stress shows stress channeling which means that the stress distribution is cubic rather than linear towards the surfaces.

puted by the developed Hellinger-Reissner model and the 3D FE model are assessed by means of the residual within Cauchy's polar equilibrium equations.

2. Theory

2.1. Derivation of the governing equations

Figure 2 shows a curved beam element with constant curvature. We use a polar coordinate system with hoop coordinate φ and radial coordinate r to derive the higher-order curved beam model. R denotes the mid-plane radius and t the thickness of the beam. The local through-thickness coordinate z is calculated as $z = r - R$ and the differential increment is $dz = dr$. In this section the derivation of the governing equations of the higher-order beam model for curved beams is described. The procedure outlined herein is similar to the one found in [16] for flat beams.

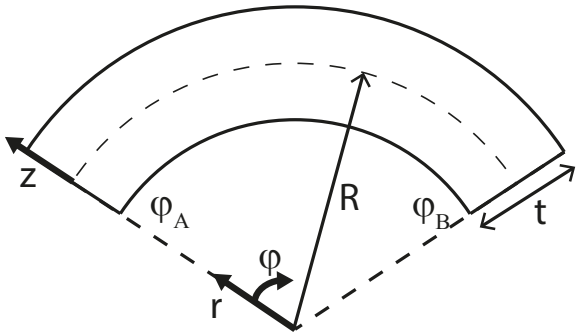

Figure 2: Definition of a curved beam element.

As illustrated in figure 3, the beam is loaded with prescribed shear and normal tractions $\hat{T}_t$ in the hoop φ direction and $\hat{P}_t$ in the radial r-direction on the top surface, and $\hat{T}_b$ and $\hat{P}_b$ on the bottom surface. These prescribed tractions can vary with φ. Additionally the beam may be loaded by a hoop stress or hoop displacement, and a transverse shear stress or transverse displacement at the two ends φ_A and φ_B of the beam. The presented model is an equivalent single layer model and hence the boundary conditions at the ends of the beam cannot be imposed layer-wise. Therefore, all the applied traction or displacement boundary conditions act through the whole beam thickness.

Figure 4 shows the convention of naming the layers. The positions of the layers are numbered starting with t_0 at the bottom at $z = -t/2$ and ending at the top with t_N at $z = t/2$. Layer k is limited by t_{k-1} to t_k. The layers

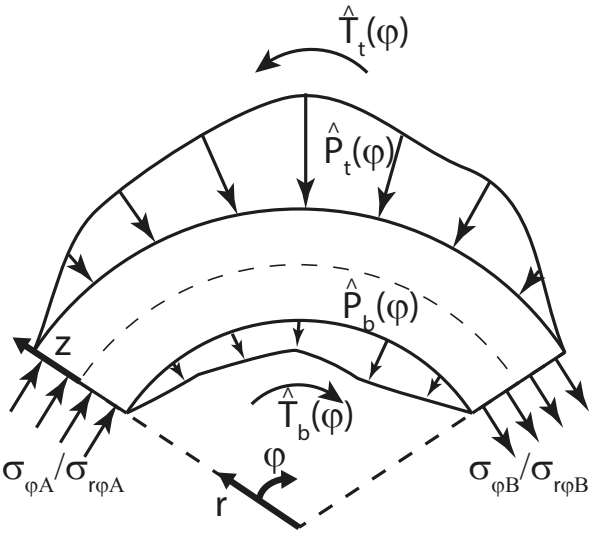

Figure 3: Loads on the beam element.

are numbered from 1 to N. In this study we choose the mid-plane of the beam as the reference plane.

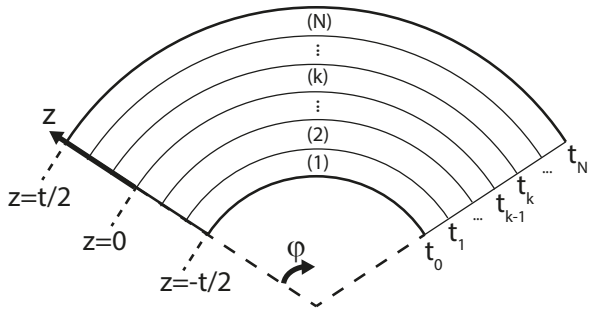

Figure 4: Layerwise notation.

2.1.1. Derivation of stress fields in polar coordinates

The displacements u_φ and u_r in the φ- and r-directions, respectively, are assumed to be of the form:

$$\begin{aligned} u_\varphi(r,\varphi) &= u_0(\varphi) + (r-R)u_1(\varphi) + \textstyle\sum_{i=2}^{n} P_n(r-R)u_i(\varphi) \\ &= \textstyle\sum_{i=0}^{n} P_n(r-R)u_i(\varphi) \\ &= \mathbf{f}^T(r-R)u_i(\varphi) \\ u_r(\varphi) &= w_0(\varphi) \end{aligned} \tag{1}$$

where $P_n(r-R)$ denotes the n^{th} Legendre polynomial, n is the modeling order and superscript T represents the matrix transpose operator. The displacement $u_r(\varphi)$ is assumed to be independent of r in order to improve the computational efficiency by reducing the number of degrees of freedom. The vector $\mathbf{f}^T(r-R) = [1\ ;\ P_i(r-R)\ ;\ \dots]$ is a vector of shape functions that describes the higher-order variation of the hoop displacement through the thickness of the beam. As shown in the following derivation, this vector of Legendre shape functions also describes the variation of the hoop strain and hoop stress through the thickness of the curved beam. The model contains n as a parameter meaning that the modeling order can be chosen arbitrarily. Due to the orthogonality of individual Legendre polynomials, all displacement variables, and hence all associated stress resultants, are independent such that it is possible to investigate the influence of each stress resultant on the stress state individually (which is not true for simple monomials). For $n = 1$ the model corresponds to the Timoshenko beam theory. The present derivation is restricted to 2D beams, but may readily be extended to a 3D curved plate model using the formulation presented in [19]. Zig-zag effects [20] are not captured in the model, hence laminations with big differences in transverse shear moduli may result in larger errors.

The strain component ϵ_φ^G is calculated from the kinematic relation:

$$\begin{aligned}\epsilon_\varphi^G &= \tfrac{1}{r}(u_{\varphi,\varphi} + u_r)\\ &= \tfrac{1}{r}[1\ P_i(r-R)\ \dots][(u_{0,\varphi}+w_0)\ u_{i,\varphi}\ \dots]^T\\ &= \tfrac{1}{r}\mathbf{f}^T(r-R)\epsilon\\ &= \tfrac{1}{z+R}\mathbf{f}^T(z)\epsilon\end{aligned} \tag{2}$$

where the superscript G refers to the fact that the strain is calculated from geometric kinematics, and $\epsilon = [(u_{0,\varphi}+w_0)\ u_{i,\varphi}\ ...]^T$ is a vector of mid-plane hoop strains.

The generalized Hooke's law for plane stress in the radial r-direction is:

$$\sigma_{ij}^{Hooke} = \bar{Q}_{ijkl}\epsilon_{kl}^G \tag{3}$$

where $\bar{Q}_{ijkl}$ is the reduced stiffness matrix, which for a curved beam can take values of plane strain or plane stress in the axial x-direction (into the page of figure 2). Using the constitutive equation (3), the hoop stress component σ_φ is expressed in terms of stress resultants. The advantage of this compared to using the displacement variables in ϵ is that the order of the greatest derivative is decreased by one, and this helps to reduce the numerical error when solving the ensuing governing differential equations.

The stress resultant vector $\mathcal{F}$ is derived from ϵ_φ^G as follows:

$$\begin{aligned}\mathcal{F} &= \int_{r_0}^{r_N} \tfrac{1}{r}\mathbf{f}(z)\sigma_\varphi^{Hooke} r dr\\ &= \int_{-t/2}^{t/2} \mathbf{f}(z)\bar{Q}^{(k)}\epsilon_\varphi^G dz\\ &= \int_{-t/2}^{t/2} \tfrac{1}{z+R}\mathbf{f}(z)\bar{Q}^{(k)}\mathbf{f}^T(z)dz\epsilon\\ &= \mathbf{S}\epsilon\end{aligned} \tag{4}$$

where the stress resultant vector is:

$$\mathcal{F} = [N_\varphi\ M_\varphi\ L_\varphi\ O_\varphi\ \dots]^T \tag{5}$$

and $\mathbf{S} = \int_{-t/2}^{t/2} \frac{1}{z+R}\mathbf{f}(z)\bar{Q}^{(k)}\mathbf{f}^T(z)dz$ is a higher-order constitutive matrix similar to the ABD matrix known from the classical lamination theory, but containing higher-order terms to account for the higher-order moments. N_φ and M_φ denote the classical membrane force and bending moment, respectively, and $L_\varphi, O_\varphi, \dots$ are higher-order moments. The superscript (k) refers to the material properties of the k^{th} of N layers of the laminate. The significance of the higher-order moments is that they capture the increasing channeling of stresses towards the outer surfaces of the beam as either the thickness or material orthotropy increases.

The hoop membrane force N_φ, transverse shear force Q_φ and hoop bending moment M_φ are defined as in classical theories:

$$\begin{aligned}N_\varphi &= \int_{-t/2}^{t/2} \sigma_\varphi dz\\ Q_\varphi &= \int_{-t/2}^{t/2} \sigma_{r\varphi} dz\\ M_\varphi &= \int_{-t/2}^{t/2} z\sigma_\varphi dz.\end{aligned} \tag{6}$$

Inverting equation (4) we find:

$$\epsilon = \mathbf{s}\mathcal{F},\ \text{with}\ \mathbf{s} = \mathbf{S}^{-1} \tag{7}$$

where $\mathbf{s}$ is the compliance matrix.

Using equation (7) and $\epsilon_\varphi = \frac{1}{z+R}\mathbf{f}^T(z)\epsilon$ from equation (2), we obtain for σ_φ:

$$\sigma_\varphi = \bar{Q}^{(k)}\epsilon_\varphi^G = \bar{Q}^{(k)}\frac{1}{z+R}\mathbf{f}^T(z)\mathbf{s}\mathcal{F} = \bar{Q}^{(k)}\frac{1}{r}\mathbf{f}^T(r-R)\mathbf{s}\mathcal{F}. \tag{8}$$

With σ_φ of equation (8) and Cauchy's polar equilibrium equations we can derive equilibrated expressions for the stress fields σ_r and $\sigma_{r\varphi}$. By deriving the stress fields for σ_r and $\sigma_{r\varphi}$ from σ_φ, the unknown variables are shared between all stress fields and the computational efficiency of the model is increased. Cauchy's equilibrium equations in polar coordinates are [21]:

$$\sigma_{r\varphi,r} + \frac{1}{r}\left(2\sigma_{r\varphi} + \sigma_{\varphi,\varphi}\right) = 0 \tag{9}$$

$$\sigma_{r,r} + \frac{1}{r}\left(\sigma_r - \sigma_\varphi + \sigma_{r\varphi,\varphi}\right) = 0. \tag{10}$$

Rearranging equation (9), we find the first-order differential equation:

$$\sigma_{r\varphi,r} + \frac{2}{r}\sigma_{r\varphi} = -\frac{1}{r}\sigma_{\varphi,\varphi} \tag{11}$$

where $\sigma_{\varphi,\varphi}$ is a known function of r that is given by the derivative of equation (8). The homogeneous part of equation (11) is:

$$\sigma^H_{r\varphi,r} + \frac{2}{r}\sigma^H_{r\varphi} = 0 \tag{12}$$

which is a first-order Euler differential equation that can be solved with the assumption $\sigma^H_{r\varphi} = r^\alpha$, where superscript H refers to the homogeneous solution. The homogeneous solution is:

$$\begin{aligned} & \alpha r^{\alpha-1} + \left(\tfrac{2}{r}\right) r^\alpha = 0 \\ \Leftrightarrow \quad & (\alpha+2)\, r^{\alpha-1} = 0 \\ \therefore \quad & \sigma^H_{r\varphi} = r^{-2}. \end{aligned} \tag{13}$$

The inhomogeneous solution can be found using the variation of parameters with the assumption $\sigma^P_{r\varphi} = C(r)\sigma^H_{r\varphi}$. Re-substituting the assumption in the original equation (11), we find the constant $C(r)$:

$$C(r) = -\int r\sigma_{\varphi,\varphi} dr \tag{14}$$

such that the solution of differential equation (9) is:

$$\begin{aligned} \sigma_{r\varphi} &= \sigma^H_{r\varphi} + \sigma^P_{r\varphi} = \sigma^H_{r\varphi} + C(r)\sigma^H_{r\varphi} \\ &= r^{-2}\left(1 - \int r\sigma_{\varphi,\varphi} dr\right) \\ &= (z+R)^{-2}\left(1 - \int (z+R)\,\sigma_{\varphi,\varphi} dz\right). \end{aligned} \tag{15}$$

The boundary conditions that are used to find the constants of integration for the last term in equation (15) are taken from the condition of interlaminar and surface traction equilibrium. These are:

- $\sigma^{(k)}_{r\varphi}(z = t_{k-1}) = \sigma^{(k-1)}_{r\varphi}(z = t_{k-1})$, i.e. interlaminar traction continuity.
- $\sigma^{(1)}_{r\varphi}(z = -t/2) = \hat{T}_b$, i.e. bottom surface traction equilibrium.
- $\sigma^{(N)}_{r\varphi}(z = t/2) = \hat{T}_t$, i.e. top surface traction equilibrium.

Hence, we have a total of $N + 1$ boundary conditions with only N conditions to be applied for each of the N layers. As shown in [16] for flat beams, when enforcing the interlaminar continuity and bottom surface equilibrium conditions explicitly, the boundary condition on the top surface is automatically fulfilled if Cauchy's hoop equilibrium equation (9) is enforced in the variational statement that is used to derive the governing equations. In Appendix A it is shown that the top surface traction boundary condition $\sigma^{(N)}_{r\varphi}(z = t/2) = \hat{T}_t$ is indeed automatically recovered if Cauchy's hoop equilibrium equation (9) is satisfied by the model.

We can now substitute equation (8) into (15) to give:

$$\begin{aligned} \sigma_{r\varphi} &= \tfrac{1}{r^2}\left(1 - \int r\bar{Q}^{(k)}\mathbf{f}^T \tfrac{1}{r}\mathbf{s}\mathcal{F}_{,\varphi} dr\right) \\ &= \tfrac{1}{(z+R)^2}\left(1 - \bar{Q}^{(k)}\int \mathbf{f}^T dz \mathbf{s}\mathcal{F}_{,\varphi}\right) \\ &= \tfrac{1}{(z+R)^2}\left(1 - \bar{Q}^{(k)}\mathbf{g}^T\mathbf{s}\mathcal{F}_{,\varphi} + a^{(k)}\right) \end{aligned} \tag{16}$$

where we define $\mathbf{g}^T = \int \mathbf{f}^T(z) dz$ which describes the through-thickness variation of the transverse shear stress. Using the interlaminar and bottom surface boundary conditions we find the integration constants $a^{(k)}$ to be:

$$\begin{aligned} a^{(k)} &= \textstyle\sum_{i=1}^{k}\left[\left(\bar{Q}^{(i)} - \bar{Q}^{(i-1)}\right)\mathbf{g}^T(t_{i-1})\right]\mathbf{s}\mathcal{F}_{,\varphi} \\ &+ \left(-\tfrac{t}{2} + R\right)^2 \hat{T}_b - 1. \end{aligned} \tag{17}$$

Hence the expression for $\sigma_{r\varphi}$ is:

$$\begin{aligned} \sigma_{r\varphi} &= \tfrac{1}{(z+R)^2}\left[-\bar{Q}^{(k)}\mathbf{g}^T\mathbf{s}\mathcal{F}_{,\varphi}\right. \\ &+ \textstyle\sum_{i=1}^{k}\left\{\left(\bar{Q}^{(i)} - \bar{Q}^{(i-1)}\right)\mathbf{g}^T(t_{i-1})\right\}\mathbf{s}\mathcal{F}_{,\varphi} \\ &+ \left.\left(-\tfrac{t}{2} + R\right)^2 \hat{T}_b\right]. \end{aligned} \tag{18}$$

In the same manner we can derive an expression for σ_r using equation (10). Rearranging equation (10) we find the following first-order Euler differential equation:

$$r\sigma_{r,r} + \sigma_r = \sigma_\varphi - \sigma_{r\varphi,\varphi}. \tag{19}$$

Using the substitution $\sigma^H_r = r^\alpha$, the solution to the homogeneous equation $r\sigma_{r,r} + \sigma_r = 0$ is:

$$\sigma^H_r = \frac{1}{r}. \tag{20}$$

The inhomogeneous solution is found with the same approach as before, namely the variation of parameters, with the assumption $\sigma^P_r = C(r)\sigma^H_r$. Thus, substituting σ^P_r into equation (19) we find:

$$C(r) = \int \left(\sigma_\varphi - \sigma_{r\varphi,\varphi}\right) dr \tag{21}$$

such that the stress field σ_r is:

$$\begin{aligned} \sigma_r &= \sigma_r^H + \sigma_r^P = \sigma_r^H + C(r)\sigma_r^H \\ \sigma_r &= \tfrac{1}{r}\left[1 + \int \left(\sigma_\varphi - \sigma_{r\varphi,\varphi}\right) dr\right]. \end{aligned} \tag{22}$$

The interlaminar and surface traction boundary conditions that are used to find the integration constants of the last term in equation (22) are:

- $\sigma_r^{(k)}(z = t_{k-1}) = \sigma_r^{(k-1)}(z = t_{k-1})$, i.e. interlaminar traction continuity.
- $\sigma_r^{(1)}(z = -t/2) = \hat{P}_b$, i.e. bottom surface traction equilibrium
- $\sigma_r^{(N)}(z = t/2) = \hat{P}_t$, i.e. top surface traction equilibrium.

Substituting equation (8) and (16) into (22) gives:

$$\begin{aligned} \sigma_r &= \tfrac{1}{(z+R)}\Big(1 + \int \Big[\bar{Q}^{(k)}\mathbf{f}^T \tfrac{1}{(z+R)}\mathbf{s}\mathcal{F} \\ &- \tfrac{1}{(z+R)^2}\Big[-\bar{Q}^{(k)}\mathbf{g}^T\mathbf{s}\mathcal{F}_{,\varphi\varphi} \\ &+ \textstyle\sum_{i=1}^{k}\left\{\left(\bar{Q}^{(i)} - \bar{Q}^{(i-1)}\right)\mathbf{g}^T(t_{i-1})\right\}\mathbf{s}\mathcal{F}_{,\varphi\varphi} \\ &+ \left(-\tfrac{t}{2} + R\right)^2 \hat{T}_{b,\varphi}\Big]\Big] dz\Big) \\ \sigma_r &= \tfrac{1}{(z+R)}\Big(1 + \bar{Q}^{(k)}\mathbf{h}^T\mathbf{s}\mathcal{F} + \bar{Q}^{(k)}\mathbf{m}^T\mathbf{s}\mathcal{F}_{,\varphi\varphi} \\ &+ \tfrac{1}{(z+R)}\textstyle\sum_{i=1}^{k}\left\{\left(\bar{Q}^{(i)} - \bar{Q}^{(i-1)}\right)\mathbf{g}^T(t_{i-1})\right\}\mathbf{s}\mathcal{F}_{,\varphi\varphi} \\ &+ \tfrac{1}{(z+R)}\left(-\tfrac{t}{2} + R\right)^2 \hat{T}_{b,\varphi} + b^{(k)}\Big) \end{aligned} \tag{23}$$

where we define $\mathbf{h}^T(z) = \int \frac{1}{(z+R)}\mathbf{f}^T(z)dz$ and $\mathbf{m}^T(z) = \int \frac{1}{(z+R)^2}\mathbf{g}^T(z)dr$. Using the interlaminar and bottom surface boundary conditions we find the integration constants $b^{(k)}$:

$$\begin{aligned} b^{(k)} &= \left(-\tfrac{t}{2} + R\right)\hat{P}_b - \left(-\tfrac{t}{2} + R\right)\hat{T}_{b,\varphi} - 1 \\ &- \textstyle\sum_{i=1}^{k}\Big[\left(\bar{Q}^{(i)} - \bar{Q}^{(i-1)}\right)\mathbf{h}^T(t_{i-1})\mathbf{s}\mathcal{F} \\ &+ \left(\bar{Q}^{(i)} - \bar{Q}^{(i-1)}\right)\mathbf{m}^T(t_{i-1})\mathbf{s}\mathcal{F}_{,\varphi\varphi} \\ &+ \tfrac{1}{t_{i-1}+R}\left(\bar{Q}^{(i)} - \bar{Q}^{(i-1)}\right)\mathbf{g}^T(t_{i-1})\mathbf{s}\mathcal{F}_{,\varphi\varphi}\Big]. \end{aligned} \tag{24}$$

Hence the expression for σ_r is:

$$\begin{aligned} \sigma_r &= \tfrac{1}{(z+R)}\Big[\bar{Q}^{(k)}\mathbf{h}^T\mathbf{s}\mathcal{F} + \bar{Q}^{(k)}\mathbf{m}^T\mathbf{s}\mathcal{F}_{,\varphi\varphi} \\ &+ \tfrac{1}{(z+R)}\textstyle\sum_{i=1}^{k}\left(\bar{Q}^{(i)} - \bar{Q}^{(i-1)}\right)\mathbf{g}^T(t_{i-1})\mathbf{s}\mathcal{F}_{,\varphi\varphi} \\ &+ \tfrac{1}{(z+R)}\left(-\tfrac{t}{2} + R\right)^2 \hat{T}_{b,\varphi} + \left(-\tfrac{t}{2} + R\right)\left(\hat{P}_b - \hat{T}_{b,\varphi}\right) \\ &- \textstyle\sum_{i=1}^{k}\Big\{\left(\bar{Q}^{(i)} - \bar{Q}^{(i-1)}\right)\mathbf{h}^T(t_{i-1})\mathbf{s}\mathcal{F} \\ &+ \left(\bar{Q}^{(i)} - \bar{Q}^{(i-1)}\right)\mathbf{m}^T(t_{i-1})\mathbf{s}\mathcal{F}_{,\varphi\varphi} \\ &+ \tfrac{1}{(t_{i-1}+R)}\left(\bar{Q}^{(i)} - \bar{Q}^{(i-1)}\right)\mathbf{g}^T(t_{i-1})\mathbf{s}\mathcal{F}_{,\varphi\varphi}\Big\}\Big] \end{aligned} \tag{25}$$

Appendix A shows that the top surface traction boundary condition $\sigma_r^{(N)}(z = t/2) = \hat{P}_t$ is automatically guaranteed, even though it was not enforced explicitly if Cauchy's radial equilibrium equation (10) is satisfied by the model.

2.1.2. Integration of Cauchy's polar equilibrium equations

In the Hellinger-Reissner mixed variational formulation, Cauchy's equilibrium equations are added as constraint conditions to the strain energy written in complementary form, i.e. in terms of stresses. This procedure enforces the equilibrium of stresses in a variational sense, and specifically in the present work guarantees that the traction boundary conditions on the top surface is recovered accurately. The strain energy is calculated by means of a volume integral, but as the present model is an equivalent single-layer theory the equilibrium equations need to be converted into a form where they can be expressed in terms of the unknown stress resultants $\mathcal{F}$. Thus, to compress Cauchy's polar equilibrium equations (9) and (10) onto an equivalent single layer, the equilibrium equations are integrated in the z-direction and combined with equation (6).

Integrating equation (9) in the z-direction leads to:

$$\begin{aligned} &\left(1 + \tfrac{t}{2R}\right)\left(R + \tfrac{t}{2}\right)\hat{T}_t - \left(1 - \tfrac{t}{2R}\right)\left(R - \tfrac{t}{2}\right)\hat{T}_b \\ &+ \tfrac{1}{R}M_{\varphi,\varphi} + N_{\varphi,\varphi} = 0 \end{aligned} \tag{26}$$

and integrating equation (10) gives:

$$\begin{aligned} &\left(\tfrac{t}{2} + R\right)\hat{P}_t - \left(-\tfrac{t}{2} + R\right)\hat{P}_b - N_\varphi \\ &+ \tfrac{1}{R}\left[\tfrac{t}{2}\left\{\left(R + \tfrac{t}{2}\right)\hat{T}_{t,\varphi} + \left(R - \tfrac{t}{2}\right)\hat{T}_{b,\varphi}\right\} + M_{\varphi,\varphi\varphi}\right] = 0. \end{aligned} \tag{27}$$

Detailed derivations of these equations are given in Appendix B.

2.2. Hellinger-Reissner mixed variational statement

To obtain the equilibrium of the system, the first variation of the potential energy functional Π:

$$\Pi(\lambda,\mathcal{F}) = \Pi_r(\mathcal{F})+\Pi_\varphi(\mathcal{F})+\Pi_{r\varphi}(\mathcal{F})+\Pi_\Gamma(\mathcal{F})+\Pi_\lambda(\lambda,\mathcal{F}) \tag{28}$$

must vanish. Hence:

$$\delta\Pi = 0 \tag{29}$$

where Π_r, Π_φ and $\Pi_{r\varphi}$ denote the complementary strain energy of the stress terms in the r-, φ- and $r\varphi$-directions, respectively. Π_Γ represents the potential energy due to the loads acting on boundary $\Gamma = (z \times \varphi_A) \cup (z \times \varphi_B)$, and Π_λ is the Lagrange multiplier potential associated with the equivalent single-layer equilibrium equations (26) and (27) multiplied by two Lagrange multipliers λ_1 and λ_2.

In this work we assume that the radial displacement $u_r(\varphi)$ is independent of r with associated negligible radial strains. Therefore, the strain energy in the radial direction is also negligible compared to the hoop and transverse shear strain energy . As a result, $\Pi_r = 0$ and equation (28) simplify to:

$$\begin{aligned}
\Pi &= \Pi_\varphi + \Pi_{r\varphi} + \Pi_\Gamma + \Pi_\lambda \\
&= \tfrac{1}{2}\int_V \sigma_\varphi \epsilon_\varphi dV + \tfrac{1}{2}\int_V \sigma_{r\varphi}\epsilon_{r\varphi} dV \\
&- \int_\Gamma \left(\sigma_\varphi \hat{u}_\varphi^{(k)} + \sigma_{r\varphi}\hat{w}_0\right) d\Gamma \\
&+ \int \lambda_1 \left[\left(1+\tfrac{t}{2R}\right)\left(R+\tfrac{t}{2}\right)\hat{T}_t - \left(1-\tfrac{t}{2R}\right)\left(R-\tfrac{t}{2}\right)\hat{T}_b \right. \\
&+ \left. \tfrac{1}{R}M_{\varphi,\varphi} + N_{\varphi,\varphi}\right] d\varphi \\
&+ \int \lambda_2 \left[\left(\tfrac{t}{2}+R\right)\hat{P}_t - \left(-\tfrac{t}{2}+R\right)\hat{P}_b - N_\varphi \right. \\
&+ \left. \tfrac{1}{R}\left\{\tfrac{t}{2}\left(\left(R+\tfrac{t}{2}\right)\hat{T}_{t,\varphi} + \left(R-\tfrac{t}{2}\right)\hat{T}_{b,\varphi}\right) + M_{\varphi,\varphi\varphi}\right\}\right] d\varphi
\end{aligned} \tag{30}$$

where a superimposed hat $\hat{}$ denotes prescribed quantities. Even though the strain energy in the radial direction Π_r is ignored, the radial stress can readily be recovered from Cauchy's equilibrium using equation (25) once $\mathcal{F}$ has been determined.

As Π_φ and $\Pi_{r\varphi}$ must be written in complementary form, the hoop strain ϵ_φ and transverse shear strain $\epsilon_{r\varphi}$ need to be replaced by the associated stresses σ_φ and $\sigma_{r\varphi}$, respectively. Thus, the hoop shear strain is replaced with $\epsilon_\varphi = \frac{1}{z+R}\mathbf{f}^T(z)\mathbf{s}\mathcal{F}$ and the transverse shear strain $\epsilon_{r\varphi}$ is replaced by the constitutive law:

$$\begin{aligned}
\epsilon_{r\varphi}^{(k)} &= \tfrac{1}{G_{r\varphi}^{(k)}}\sigma_{r\varphi}^{(k)} \\
&= \tfrac{1}{G_{r\varphi}^{(k)}}\tfrac{1}{r^2}\left(1 - \bar{Q}^{(k)}\mathbf{g}^T\mathbf{s}\mathcal{F}_{,\varphi} + a^{(k)}\right).
\end{aligned} \tag{31}$$

Hence, the total potential energy Π is written in terms of the stress resultants $\mathcal{F}$ and Lagrange multipliers λ_1 and λ_2 only, which are the functional unknowns of the theory. Each individual term of equation (30) is elucidated in more detail in Appendix C.

To find the resulting governing equations, the first variation of the potential energy in equation (30) is found via the calculus of variations. The detailed derivations of this step are reported in Appendix D. The resulting Euler-Lagrange integral equations over the domain φ of the curved beam are the governing field equations of the model, whereas the Euler-Lagrange boundary equations resulting from integration by parts are the pertinent boundary conditions.

The governing field equations comprise $n+1$ stress-displacement equations related to the variations of the stress resultants $\delta\mathcal{F}^T = [\delta N \ \delta M \ \dots]$, and two equivalent single-layer equilibrium equations (26) and (27) related to the variations of the Lagrange multipliers $\delta\lambda_1$ and $\delta\lambda_2$. Hence:

$$\begin{aligned}
\delta\mathcal{F}^T: \quad & \mathbf{s}\mathcal{F} - \left(\eta^T\mathcal{F}_{,\varphi\varphi} + \chi\left(R-\tfrac{t}{2}\right)^2\hat{T}_{b,\varphi}\right) + \mathbf{\Lambda}_{HR} = \mathbf{0} \\
\delta\lambda_1: \quad & \left(1+\tfrac{t}{2R}\right)\left(R+\tfrac{t}{2}\right)\hat{T}_t - \left(1-\tfrac{t}{2R}\right)\left(R-\tfrac{t}{2}\right)\hat{T}_b \\
& + \tfrac{1}{R}M_{\varphi,\varphi} + N_{\varphi,\varphi} = 0 \\
\delta\lambda_2: \quad & \left(\tfrac{t}{2}+R\right)\hat{P}_t - \left(-\tfrac{t}{2}+R\right)\hat{P}_b - N_\varphi \\
& + \tfrac{1}{R}\left[\tfrac{t}{2}\left\{\left(R+\tfrac{t}{2}\right)\hat{T}_{t,\varphi} + \left(R-\tfrac{t}{2}\right)\hat{T}_{b,\varphi}\right\}\right. \\
& \left. + M_{\varphi,\varphi\varphi}\right] = 0
\end{aligned} \tag{32}$$

where:

$$\mathbf{\Lambda}_{HR} = \begin{bmatrix} -\lambda_{1,\varphi} - \lambda_2 \\ -\frac{1}{R}\lambda_{1,\varphi} + \frac{1}{R}\lambda_{2,\varphi\varphi} \\ 0 \\ \vdots \\ 0 \end{bmatrix} \tag{33}$$

and η and χ are matrices of shear correction factors defined in equation (C.6). Besides the classical membrane and bending equilibrium equations associated with $\delta\lambda_1$ and $\delta\lambda_2$ in equation (32), respectively, the governing equations related to $\delta\mathcal{F}^T$ represent the higher-order relation between stress resultants $\mathcal{F}$ and mid-plane membrane strains and curvatures $\mathbf{\Lambda}_{HR}$, and are therefore higher-order stress-displacement relations.

The natural (stress) and essential (displacement)

boundary conditions are:

$$\delta\mathcal{F}^T = 0 \quad \text{or} \quad \eta^T\mathcal{F}_{,\varphi} + \chi\left(R - \tfrac{t}{2}\right)^2 \hat{T}_b + \mathbf{\Lambda}_{BC1} = \hat{\mathcal{U}}_\varphi$$
$$\delta\mathcal{F}^T_{,\varphi} = 0 \quad \text{or} \quad \mathbf{\Lambda}_{BC2} = \hat{W} \tag{34}$$

where:

$$\mathbf{\Lambda}_{BC1} = \begin{bmatrix} \lambda_1 \\ \frac{1}{R}\lambda_1 - \frac{1}{R}\lambda_{2,\varphi} \\ 0 \\ \vdots \\ 0 \end{bmatrix}, \ \mathbf{\Lambda}_{BC2} = \begin{bmatrix} 0 \\ \lambda_2 \\ 0 \\ \vdots \\ 0 \end{bmatrix}, \ \hat{W} = \begin{bmatrix} 0 \\ \hat{w}_0 \\ 0 \\ \vdots \\ 0 \end{bmatrix} \tag{35}$$

and $\hat{\mathcal{U}}_\varphi = (\hat{u}_0 \ \hat{u}_1 \ \ldots)^T$ and $\hat{w}_0$ are the prescribed mid-plane hoop and transverse displacements, respectively, at the two ends φ_A and φ_B of the curved beam.

The governing equations are thus ordinary differential equations of φ, which can be solved for the unknown components of the stress resultants $\mathcal{F}$ (which are needed to calculate the stress fields), and the two Lagrange multipliers λ_1 and λ_2. Equations (34) and (35) also show the significance of the two Lagrange multipliers; λ_1 is equal to the mid-plane hoop displacement u_0 and λ_2 equals the transverse displacement w_0. The governing equations are much less complex than for 3D finite element formulations and hence can be solved with little numerical effort.

2.3. Differential quadrature method

To solve the governing equations and the related boundary conditions in their strong form the differential quadrature method (DQM) is used. It has been previously shown that DQM is an efficient strategy for solving the stretching and bending problems [22, 23] of composite laminates.

DQM is a pseudo-spectral method, which replaces the derivatives of a function with a linear weighting matrix, $A^{(m)}_{ij}$, multiplied by all functional values within the domain [24]:

$$\frac{d^m f(\varphi_i)}{d\varphi^m} = \sum_{i=1}^{N_p} A^{(m)}_{ij} f(\varphi_j) \tag{36}$$

where m is the order of the derivative and N_p is the number of grid points. In the examples that are shown in this study the numerical solution converged for $N_p = 11$. DQM is a collocation method by which the residual between the numerical solution and an exact solution is equal to zero at the grid points assuming that the numerical inversion of the algebraic equations occurs without numerical errors. Between the grid points it cannot be guaranteed that the residual is exactly equal to zero. In the present work the Lagrangian polynomial weighting matrix based on the non-uniform Chebychev-Gauss-Labatto grid is used [24] which was shown to give excellent numerical convergence and stability properties. The Chebychev-Gauss-Labatto points result in minimum descretisation errors. By biasing grid points towards the boundaries Runge phenomena are avoided and the interpolation error reduces with increasing polynomial order. Hence, by replacing all the derivatives with the weighting matrix and the functional values themselves, the differential equations can be transformed to standard linear algebraic equations.

3. Results

3.1. Validation of the stress field using finite element method

To validate the model the results for a number of different loading cases are compared with a high fidelity 3D FE model. The FE model is carried out in Ansys classic 14.5 and consists of 512,000 SOLID186 elements with 16 elements through the thickness (4 elements per layer), 160 elements along the circumference, and 200 elements in the x-direction. This element is a 20 node brick element and is used as a structural solid element. A pure displacement formulation and uniform reduced integration is used. The assumed material properties are given in table 1 and are representative of the CFK T300 Epoxy material. Two different lay-ups are tested, the first is a $[0\ 0\ 0\ 0]_{deg}$ laminate and the second a $[0\ 90\ 90\ 0]_{deg}$ laminate. To ensure convergence the Hellinger-Reissner results are calculated up to a model order of $n = 9$. The curved beam is clamped at both ends and a prescribed displacement is enforced on the right edge, as shown in figure 5. The thickness of the beam is 8 mm in total, all four layers have a thickness of 2 mm. The radius of the beam is 25.6 mm and the opening angle ψ_0 is 155°. The enforced displacement w_{disp} equals 0.5 mm.

Material properties					
E_{11}[GPa]	135	E_{22}[GPa]	10	E_{33}[GPa]	10
G_{12}[GPa]	5	G_{13}[GPa]	5	G_{23}[GPa]	3.846
ν_{12} [-]	0.02	ν_{13} [-]	0.02	ν_{23} [-]	0.3

Table 1: Material properties of CFK T300 Epoxy.

All following plots of the stress distributions are calculated with a 11 point Chebychev-Gauss-Lobatto grid.

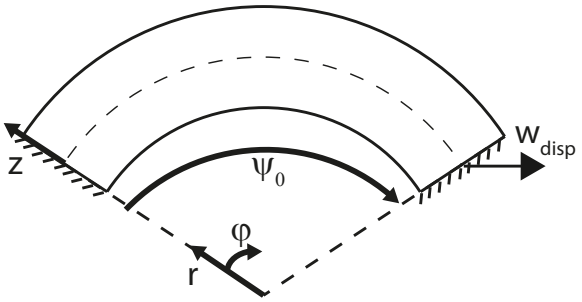

Figure 5: Geometry of the analyzed beam and applied boundary conditions.

Between the grid points the values are interpolated using Lagrange polynomials. Figures 6 to 8 show the results for the first unidirectional lay-up. The results of the Hellinger-Reissner beam model agree very well with the 3D FE model. In figure 6 we observe that the stress channeling in σ_φ (as reported by [14]) is captured robustly with the present model, underlining that higher-order terms are important. Further, figures 7 and 8 show that the continuity of transverse stresses at layer interfaces and the traction-free surfaces are fulfilled. Figures 6 to 8 show that all three stress components are predicted accurately with the Hellinger-Reissner model and the numerical effort, in comparison with the FE simulation, is significantly smaller. While the Hellinger-Reissner model solves an ordinary differential equation with one variable (φ), the FE simulation solves a three dimensional partial differential equation (x, φ, and r) in case of a high fidelity model or a two dimensional partial differential equation (φ and r) if a plane model is used. A further advantage of the Hellinger-Reissner model concerning computational time is that it directly provides stress results. In displacement-based FEM approaches the stress results are calculated in a post-processing step from the displacement solution. As the stress results are one polynomial order lower than the displacement results an FEM model requires very fine meshes through the thickness with several elements per layer to achieve accurate stress results.

Figures 9 to 11 show the comparison between the Hellinger-Reissner beam model and the 3D FE model for the second tested lay-up. Again, these results indicate the excellent agreement between the stresses predicted by the Hellinger-Reissner and the 3D FE models. Similarly, the interlaminar continuity condition and surface boundary conditions of the transverse stresses are satisfied for the Hellinger-Reissner model.

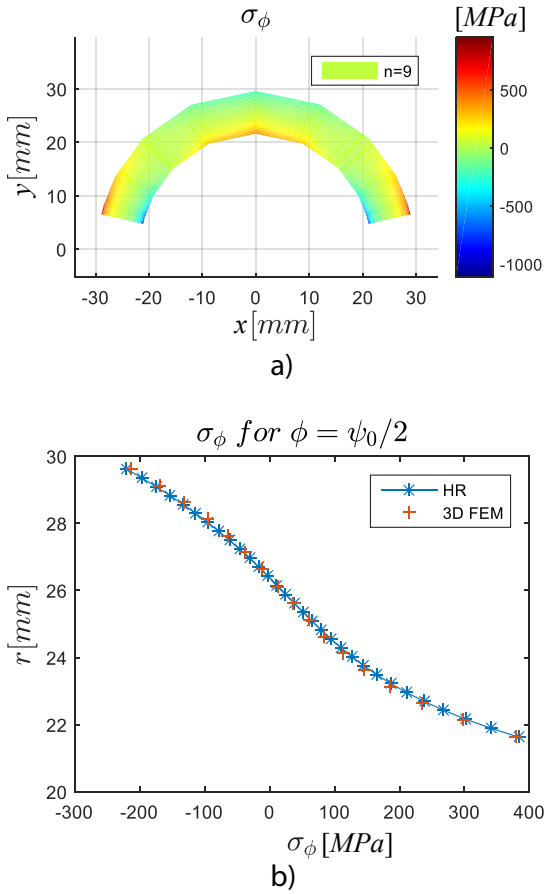

Figure 6: a) Distribution of σ_φ throughout the curved beam calculated with the Hellinger-Reissner model and b) a comparison between the Hellinger-Reissner $n = 9$ model and 3D FE results at mid-span.

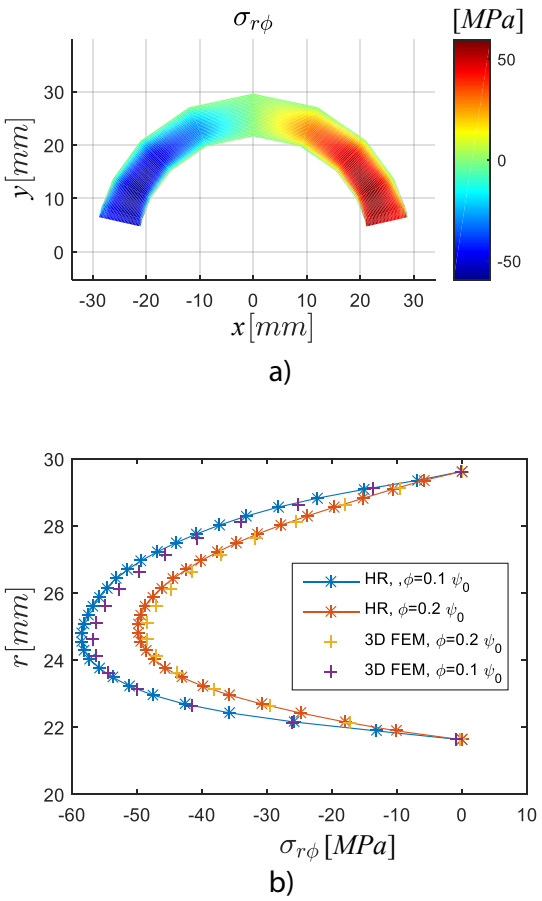

Figure 7: a) Distribution of $\sigma_{r\varphi}$ throughout the curved beam calculated with the Hellinger-Reissner model and b) a comparison between the Hellinger-Reissner $n = 9$ model and 3D FE results at 10% and 20% from the left end of the beam.

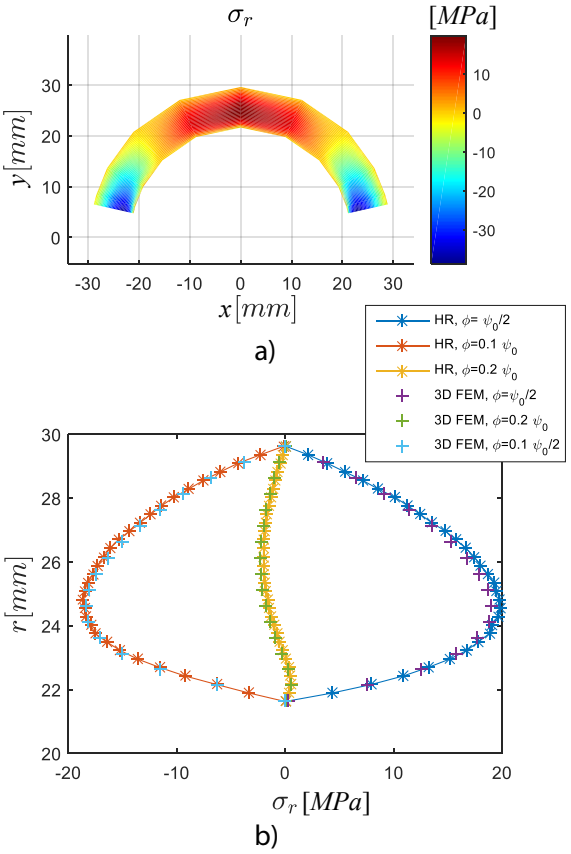

Figure 8: a) Distribution of σ_r throughout the curved beam calculated with the Hellinger-Reissner model and b) a comparison between the Hellinger-Reissner $n = 9$ model and 3D FE results at 10% and 20% from the left end of the beam and at the mid-span.

As demonstrated in [16] the approach is also valid for unsymmetrical lay-ups. The lay-up (symmetrical or unsymmetrical) does not influence the convergence behavior of the model.

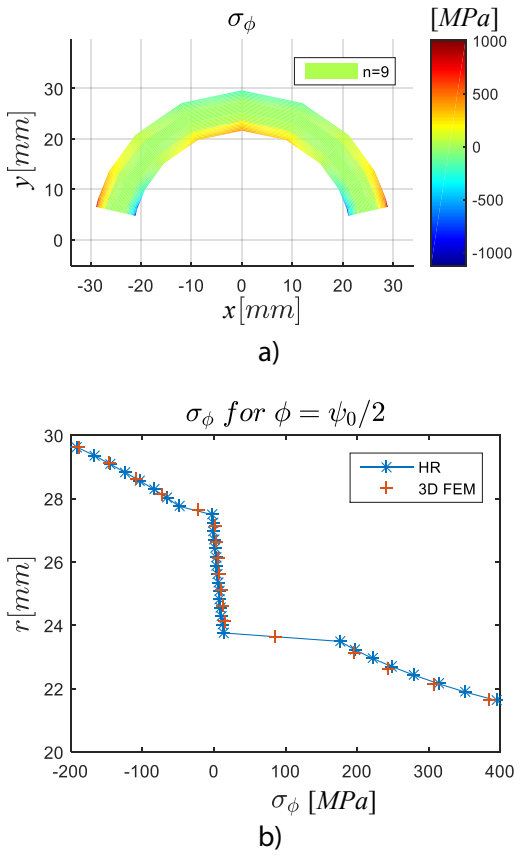

Figure 9: a) Distribution of σ_φ throughout the curved beam calculated with the Hellinger-Reissner model and b) a comparison between the Hellinger-Reissner $n = 9$ model and 3D FE results at mid-span.

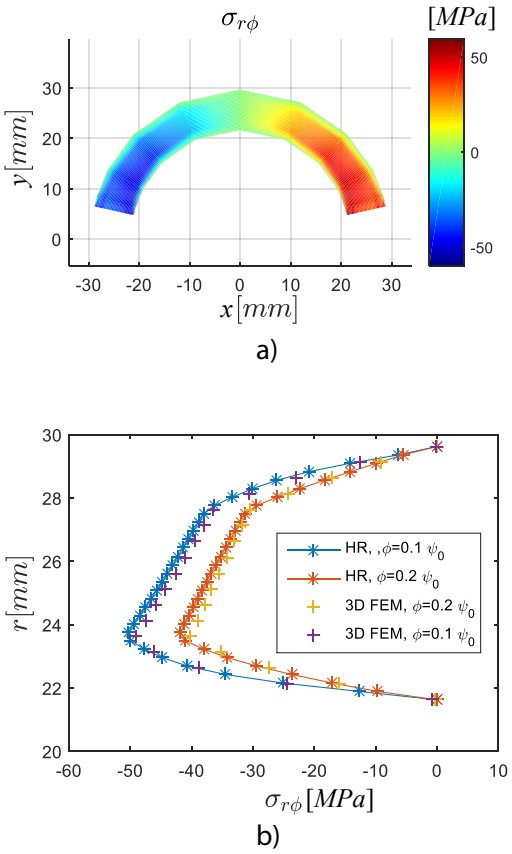

Figure 10: a) Distribution of $\sigma_{r\varphi}$ throughout the curved beam calculated with the Hellinger-Reissner model and b) a comparison between the Hellinger-Reissner $n = 9$ model and 3D FE results at 10% and 20% from the left end of the beam.

3.2. Convergence analysis

Figures 12 to 14 show a convergence analysis of the modeling order n for the first lay-up. The plots show that the results converge to the 3D FE solution for the modeling order $n = 3$ or $n = 4$. Figure 12 shows that a first- or second-order model is not able to capture higher-order effects such as stress channeling towards the surfaces in the hoop stress σ_φ. Furthermore, figures 13 and 14 show that low-order models ($n < 3$) cannot predict the stress distributions of the transverse stresses $\sigma_{r\varphi}$ and σ_r accurately. Especially for thick beams higher-order terms are needed to approach the 3D FE stress prediction.

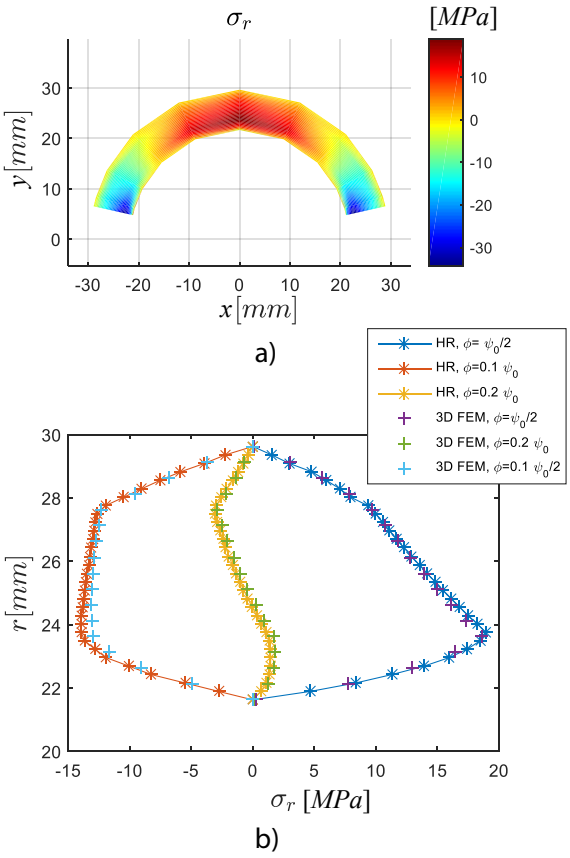

Figure 11: a) Distribution of σ_r throughout the curved beam calculated with the Hellinger-Reissner model and b) a comparison between the Hellinger-Reissner $n = 9$ model and 3D FE results at 10% and 20% from the left end of the beam and at the mid-span.

The influence of the curvature and the number of layers on the convergence was investigating by doubling the number of layers and testing different curvatures while keeping the arc-length constant. We found that the convergence behavior is not influenced by the number of layers. For increasing curvatures the results imply that slightly higher modeling orders are needed. However, all the tested examples converged for $n \leq 5$.

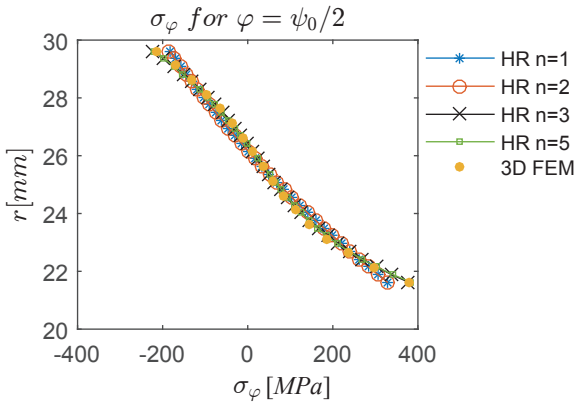

Figure 12: Convergence analysis of the Hellinger-Reissner modelling order n for σ_φ at the midspan. The curves for $n = 1, 2$ and $n = 3, 5$ respectively are overlaid with each other.

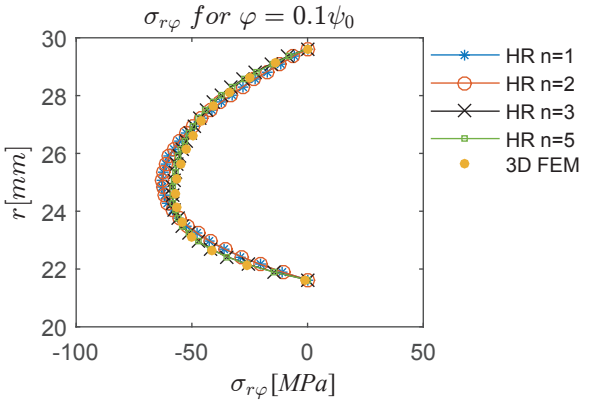

Figure 13: Convergence analysis of the Hellinger-Reissner modelling order n for $\sigma_{r\varphi}$ at 10% from the left end of the curved beam. The curves for $n = 1, 2$ and $n = 3, 5$ respectively are overlaid with each other.

3.3. Comparison with other models

Figure 15 shows a comparison between the Hellinger-Reissner models with $n = 1$ and $n = 5$, the FE solution and two first-order shear deformation theory models, namely the Timoshenko curved beam model [17]

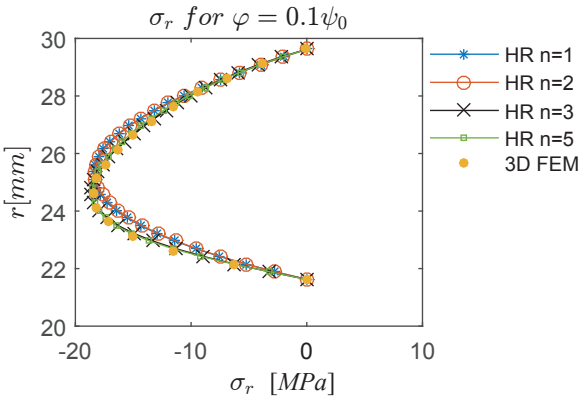

Figure 14: Convergence analysis of the Hellinger-Reissner modelling order n for σ_r at 10% from the left end of the curved beam. The curves for $n = 1, 2$ and $n = 3, 5$ respectively are overlaid with each other.

and a Lekhnitskii-type curved beam model by Kedward et al. [18]. The first-order Timoshenko and a Lekhnitskii-type curved beam models match very well with the Hellinger-Reissner model for $n = 1$. However, these models are much less accurate than the Hellinger-Reissner model for $n = 5$.

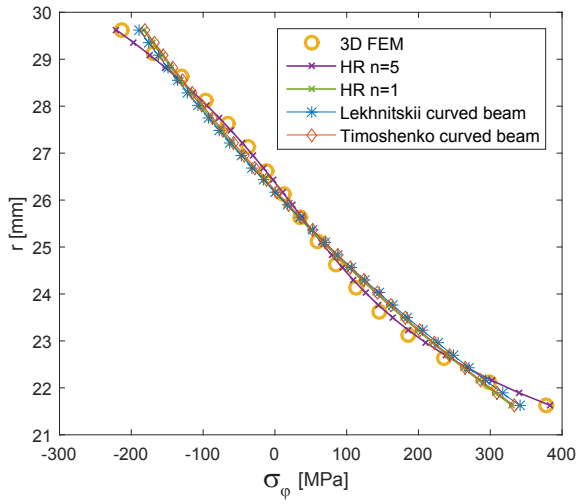

Figure 15: Hellinger-Reissner model results for σ_φ at $\varphi = \psi_0/2$ with modeling order $n = 1$ and $n = 5$ compared to 3D FE, Timoshenko curved beam [17] and Lekhnitskii-type curved beam results [18].

3.4. Stress residuals

In order to check the quality of the solution, we calculate the residuals in Cauchy's polar equilibrium equations by re-substituting the Hellinger-Reissner and 3D FE solutions into equilibrium equations (9) and (10). Equation (9) represents the hoop equilibrium and (10) the radial equilibrium. Analytical expressions for the required derivatives for the Hellinger-Reissner model are given in Appendix E. For the FE model the derivatives are calculated numerically, and hence are perhaps evaluated less accurately. The numerical algorithm to calculate the gradients is based on central differences for interior data points and single-sided differences for points along the edges. Between the data points Lagrange polynomials are used for interpolation. Figures 16 and 17 show the stress residuals for the Hellinger-Reissner beam model and the FE model, respectively. The stress residuals for the Hellinger-Reissner beam model in figure 16 are almost equal to zero, hence the equilibrium equations are fulfilled highly accurately. The stress residuals for the FE model in figure 17 are finite and multiple orders of magnitude greater than for the Hellinger-Reissner model, which indicates that the equilibrium conditions are not fulfilled as accurately by the 3D FE model. The residuals are especially pronounced at the boundaries as the equilibrium of stresses and traction boundary conditions at the clamped edges are not enforced explicitly in the weak-form displacement-based FEM, and therefore there is no guarantee that the stresses converge to meaningful values in the vicinity of the edges [25, 26]. However, figure 17 also shows that a finite residual is perpetuated even further towards the mid-span. For the Hellinger-Reissner model the residuals are also negligible close to the boundaries. This indicates that the combination of enforcing Cauchy's polar equilibrium equations explicitly in the variational statement and solving the ensuing governing differential equations in the strong-form has certain advantages for predicting accurate stress fields towards boundary conditions. This capability is particularly useful for damage analysis as delaminations and other damage phenomena typically occur in the region of boundaries where stress gradients are pronounced.

4. Conclusions

The present work has shown that accurate 3D stress fields in curved multilayered beams of arbitrary constant thickness and constant curvature can be predicted using an equivalent single-layer model derived from the Hellinger-Reissner mixed variational statement. The hoop, radial and transverse shear stresses are constructed from a generalized higher-order series of stress resultants multiplied by Legendre polynomials, and are inherently equilibrated. By expanding the stress fields

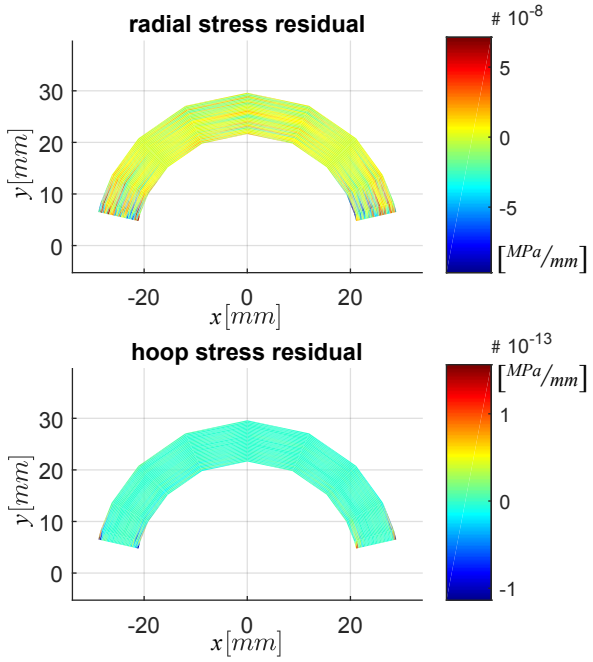

Figure 16: Residuals produced by the Hellinger-Reissner stress predictions in Cauchy's hoop and radial equilibrium equations.

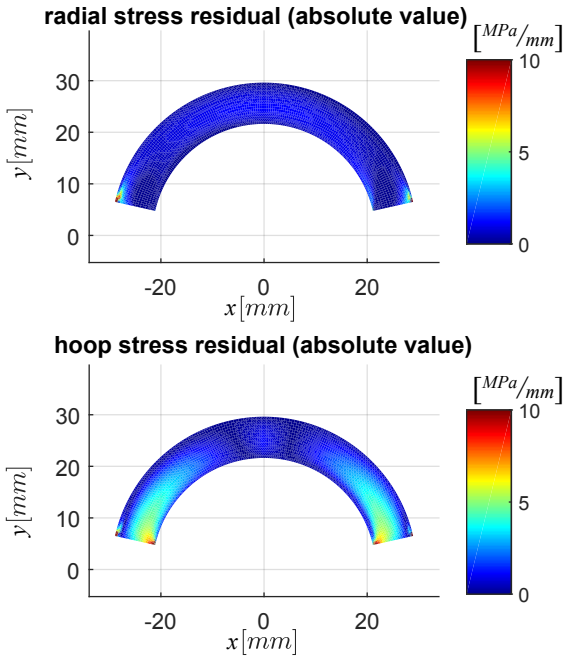

Figure 17: Residuals produced by the 3D FE stress predictions in Cauchy's hoop and radial equilibrium equations at the mid-plane, the plots show the absolute values.

in the thickness direction via orthogonal Legendre polynomials, the membrane forces, bending moments and all higher-order stress resultants are fully decoupled. Higher-order moments are needed to capture the channeling of hoop stresses towards the beam surfaces and are increasingly important for thicker beams. By using the Hellinger-Reissner mixed variational statement, new stress-displacement relations are derived which are of the form of ordinary differential equations. These equations are supplemented with the classical membrane and bending equilibrium equations of a curved beam to form the governing field equations of the theory. In the present paper the pseudo-spectral differential quadrature method is used to solve these governing equations.

The presented model predicts the hoop, radial and transverse shear stress fields in multilayered beams with high accuracy as shown. A convergence analysis of the modeling order showed that higher-order moments up to 3^{rd} or 4^{th} order are needed to guarantee accurate stress results. When considering only first-order terms, the same results as Timoshenko beam theory are obtained.

A comparison with a high fidelity 3D finite element model showed excellent agreement for all stress fields for two different laminations and at different span-wise locations. Comparisons with closed-form analytical models showed that these simpler models can be adequate for thin laminates, but that first-order shear deformation theory is not capable of capturing higher-order effects for thicker laminates. Whereas the 3D FE benchmarks provide accurate stress results, the computational costs are very high. On the contrary, closed-form analytical models allow very fast analysis, but are lacking in accuracy for thicker laminates. In relation to this, the developed Hellinger-Reissner model provides a good compromise between accurate stress predictions and little numerical effort.

In conclusion, the developed model presents a promising analysis tool for accurate stress predictions in curved beams. Future work will focus on using the presented model to investigate the onset of damage in different curved laminated structures.

Acknowledgment

The first and third authors gratefully acknowledge the support of the Swiss National Science Foundation (project no. 149200). The second and fourth authors sincerely thank the Engineering and Physical Sciences Research Council for funding through the EPSRC Centre for Doctoral Training at the Advanced Compos-

ites Centre for Innovation and Science [grant number EP/G036772/1] at the University of Bristol.

References

[1] G. Wimmer, W. Kitzmüller, G. Pinter, T. Wettemann, H. E. Pettermann, Computational and experimental investigation of delamination in L-shaped laminated composite components, Engineering Fracture Mechanics 76 (18) (2009) 2810–2820.

[2] M. R. Wisnom, M. I. Jones, Delamination due to interaction between curvature induced interlaminar tension and stresses at terminating plies, Composite Structures 32 (1-4) (1995) 615–620.

[3] J. Most, D. Stegmair, D. Petry, Error estimation between simple, closed-form analytical formulae and full-scale FEM for interlaminar stress prediction in curved laminates, Composite Structures 131 (2015) 72–81.

[4] I. Uyar, M. A. Arca, B. Gozluklu, D. Coker, Experimental Observations of Dynamic Delamination in Curved [0] and [0/90] Composite Laminates 5 (2015) 189–196.

[5] M. R. Wisnom, The role of delamination in failure of fibre-reinforced composites, Philosophical Transactions of the Royal Society A: Mathematical, Physical and Engineering Sciences 370 (1965) (2012) 1850–1870.

[6] S. Mcrobbie, A. J. Longmuir, J. Wilcox, A. G. Gibson, H. W. Chandler, Through-thickness stress in curved laminates of single- and double-skinned construction, Composite Structures 26 (5) (1995) 339–345.

[7] R. A. Shenoi, W. Wang, Through-thickness stresses in curved composite laminates and sandwich beams, Composites Science and Technology 61 (11) (2001) 1501–1512.

[8] T. Kant, K. Swaminathan, Estimation of transverse/interlaminar stresses in laminated compositesa selective review and survey of current developments, Composite structures 49 (1) (2000) 65–75.

[9] G. Kress, R. Roos, M. Barbezat, C. Dransfeld, P. Ermanni, Model for interlaminar normal stress in singly curved laminates, Composite Structures 69 (4) (2005) 458–469.

[10] R. Roos, G. Kress, M. Barbezat, P. Ermanni, Enhanced model for interlaminar normal stress in singly curved laminates, Composite Structures 80 (3) (2007) 327–333.

[11] F. Fraternali, G. Bilotti, Nonlinear elastic stress analysis in curved composite beams, Computers & Structures 62 (5) (1997) 837–859.

[12] J. M. Gonzalez-Cantero, E. Graciani, F. Paris, B. Lopez-Romano, D. Meizoso-Latova, Semi-Analytic Solution of Non-Regularized Unfolding Stresses in Composite Beams Employing a Series Approximation Based on Legendre Polynomials, in: International Conference on Composite Materials ICCM20, Copenhagen, July 19-24, (2015).

[13] W. Hao, D. Ge, Y. Ma, X. Yao, Y. Shi, Experimental investigation on deformation and strength of carbon/epoxy laminated curved beams, Polymer Testing 31 (4) (2012) 520–526.

[14] G. C. Everstine, A. C. Pipkin, Stress channelling in transversely isotropic elastic composites, Zeitschrift für angewandte Mathematik und Physik ZAMP 22 (5) (1971) 825–834.

[15] E. Carrera, Theories and finite elements for multilayered, anisotropic, composite plates and shells, Vol. 9, (2002).

[16] R. M. J. Groh, P. M. Weaver, On displacement-based and mixed-variational equivalent single layer theories for modelling highly heterogeneous laminated beams, International Journal of Solids and Structures 59 (2015) 147–170.

[17] S. Timoshenko, Theory of Elasticity, 2nd Edition, McGraw-Hill Book Company, Inc., New York, (1951).

[18] K. Kedward, R. Wilson, S. McLean, Flexure of simply curved composite shapes, Composites 20 (6) (1989) 527–536.

[19] R. Groh, P. Weaver, A computationally efficient 2D model for inherently equilibrated 3D stress predictions in heterogeneous laminated plates. Part I: Model formulation, Composite Structures, In Press, (2015).

[20] E. Carrera, Historical review of Zig-Zag theories for multilayered plates and shells, Applied Mechanics Reviews 56 (3) (2003) 287–308.

[21] J. N. Reddy, Theory and Analysis of Elastic Plates and Shells, 2nd Edition, CRC Press, New York, (2007).

[22] R. M. J. Groh, P. M. Weaver, S. C. White, G. Raju, Z. Wu, A 2D equivalent single-layer formulation for the effect of transverse shear on laminated plates with curvilinear fibres, Composite Structures 100 (2013) 464–478.

[23] R. M. J. Groh, P. M. Weaver, Full-Field Stress Tailoring of Composite Laminates, in: 20th International Conference on Composite Materials ICCM20, Copenhagen, July 19-24, (2015).

[24] C. Shu, Differential Quadrature and Its Application in Engineering, Springer, London, (2000).

[25] R. L. Spilker, A traction-free-edge hybrid-stress element for the analysis of edge effects in cross-ply laminates, Computers and Structures 12 (1979) 167–179.

[26] R. L. Spilker, S. Chou, Edge effects in symmetric composite laminates: Importance of satisfying the traction-free-edge condition, Journal of Composite Materials 14 (1980) 2–20.

Appendix A. Fulfillment of the boundary conditions

We need to check whether the shear traction equilibrium boundary condition on the top surface is accurately recovered when Cauchy's hoop equilibrium equation is satisfied. To show this, we use the integrated equilibrium condition in equation (26) and evaluate it between $-t/2$ and $t/2$. Using equation (8), the expression $\frac{1}{R}M_{\varphi,\varphi} + N_{\varphi,\varphi}$ is written as:

$$\begin{aligned}
\tfrac{1}{R}M_{\varphi,\varphi} + N_{\varphi,\varphi} &= \int_{-t/2}^{t/2}\left(\tfrac{1}{R}z\sigma_{\varphi,\varphi} + \sigma_{\varphi,\varphi}\right)dz \\
&= \int_{-t/2}^{t/2}\left(\tfrac{z}{R}+1\right)\tfrac{R}{R}\tfrac{1}{z+R}\mathbf{f}^T dz\bar{Q}^{(k)}\mathbf{s}\mathcal{F}_{,\varphi} \\
&= \int_{-t/2}^{t/2}\tfrac{1}{R}\mathbf{f}^T dz\bar{Q}^{(k)}\mathbf{s}\mathcal{F}_{,\varphi} \\
&= \tfrac{1}{R}\sum_{k=1}^{N}\left[\bar{Q}^{(k)}\mathbf{g}^T(t_k) - \bar{Q}^{(k)}\mathbf{g}^T(t_{k-1})\right]\mathbf{s}\mathcal{F}_{,\varphi}
\end{aligned} \tag{A.1}$$

and $\left(1+\frac{t}{2R}\right)\left(R+\frac{t}{2}\right)\sigma_{r\varphi}(z=\frac{t}{2})$ using equation (18) is:

$$\begin{aligned}
\left(1+\tfrac{t}{2R}\right)\left(R+\tfrac{t}{2}\right)\sigma_{r\varphi}(z=\tfrac{t}{2}) &= \tfrac{1}{R}\left(R+\tfrac{t}{2}\right)\left(R+\tfrac{t}{2}\right)\tfrac{1}{(R+t/2)^2} \\
&\quad\cdot\left(-\bar{Q}^{(N)}\mathbf{g}^T(t/2)\mathbf{s}\mathcal{F}_{,\varphi}\right. \\
&+ \sum_{i=1}^{N}\left[\bar{Q}^{(i)}\mathbf{g}^T(t_{i-1}) - \bar{Q}^{(i-1)}\mathbf{g}^T(t_{i-1})\right]\mathbf{s}\mathcal{F}_{,\varphi} \\
&+ \left.\left(R-\tfrac{t}{2}\right)^2\hat{T}_b\right) \\
&= -\tfrac{1}{R}\left(\sum_{k=1}^{N}\left[\bar{Q}^{(k)}\mathbf{g}^T(t_k) - \bar{Q}^{(k)}\mathbf{g}^T(t_{k-1})\right]\mathbf{s}\mathcal{F}_{,\varphi}\right. \\
&- \left.\left(R-\tfrac{t}{2}\right)^2\hat{T}_b\right).
\end{aligned} \tag{A.2}$$

Hence, re-substituting equation (A.1) and (A.2) into the hoop equilibrium equation (26) results in exactly zero. This shows that the shear traction equilibrium boundary condition, which was not enforced explicitly in the derivation of the integration constants of equation (17), is automatically guaranteed as long as the equilibrium equation (26) is satisfied in the model.

The same analysis is repeated for the radial equilibrium equation (27), to show that the radial traction equilibrium condition on the top surface is automatically satisfied when equilibrium equation (27) is fulfilled in the model. We use equation (B.9) and evaluate the integrals between $-t/2$ and $t/2$. For the expression $-\int\sigma_\varphi dr + \int\sigma_{r\varphi,\varphi}dr$ we write:

$$\begin{aligned}
-\int\sigma_\varphi dr + \int\sigma_{r\varphi,\varphi}dr &= -\int_{-t/2}^{t/2}\bar{Q}^{(k)}\tfrac{1}{z+R}\mathbf{f}^T dz\mathbf{s}\mathcal{F} \\
&+ \int_{-t/2}^{t/2}\tfrac{1}{(z+R)^2}\left(-\bar{Q}^{(k)}\mathbf{g}^T(z)\mathbf{s}\mathcal{F}_{,\varphi\varphi}\right. \\
&+ \sum_{i=1}^{k}\left[\left(\bar{Q}^{(i)} - \bar{Q}^{(i-1)}\right)\mathbf{g}^T(t_{i-1})\right]\mathbf{s}\mathcal{F}_{,\varphi\varphi} \\
&+ \left.\left(R-\tfrac{t}{2}\right)^2\hat{T}_{b,\varphi}\right)dz \\
&= -\sum_{k=1}^{N}\left[\bar{Q}^{(k)}\mathbf{h}^T(t_k) - \bar{Q}^{(k)}\mathbf{h}^T(t_{k-1})\right]\mathbf{s}\mathcal{F} \\
&- \sum_{k=1}^{N}\left[\bar{Q}^{(k)}\mathbf{m}^T(t_k) - \bar{Q}^{(k)}\mathbf{m}^T(t_{k-1})\right]\mathbf{s}\mathcal{F}_{,\varphi\varphi} \\
&- \sum_{k=1}^{N}\left[\tfrac{1}{t_k+R}\sum_{i=1}^{k}\left[\left(\bar{Q}^{(i)} - \bar{Q}^{(i-1)}\right)\mathbf{g}^T(t_{i-1})\right]\mathbf{s}\mathcal{F}_{,\varphi\varphi}\right. \\
&- \left.\tfrac{1}{t_{k-1}+R}\sum_{i=1}^{k-1}\left[\left(\bar{Q}^{(i)} - \bar{Q}^{(i-1)}\right)\mathbf{g}^T(t_{i-1})\right]\mathbf{s}\mathcal{F}_{,\varphi\varphi}\right] \\
&- \sum_{k=1}^{N}\left[\tfrac{1}{t_k+R} - \tfrac{1}{t_{k-1}+R}\right]\left(R-\tfrac{t}{2}\right)^2\hat{T}_{b,\varphi}.
\end{aligned} \tag{A.3}$$

For $\left(R+\frac{t}{2}\right)\sigma_r(z=t/2)$ using equation (23) we can write:

$$\begin{aligned}\left(R+\tfrac{t}{2}\right)\sigma_r(z=t/2) &= \tfrac{R+t/2}{R+t/2}\left(1+\bar{Q}^{(N)}\mathbf{h}^T(t/2)\mathbf{s}\mathcal{F}+\bar{Q}^{(N)}\mathbf{m}^T(t/2)\mathbf{s}\mathcal{F}_{,\varphi\varphi}\right.\\ &+ \tfrac{1}{R+t/2}\textstyle\sum_{i=1}^{N}\left(\bar{Q}^{(i)}-\bar{Q}^{(i-1)}\right)\mathbf{g}^T(t_{i-1})\mathbf{s}\mathcal{F}_{,\varphi\varphi}\\ &+ \left.\tfrac{1}{R+t/2}\left(R-\tfrac{t}{2}\right)^2\hat{T}_{b,\varphi}+b^{(N)}\right)\end{aligned} \tag{A.4}$$

where b_N is:

$$\begin{aligned}b^{(N)} &= \left(R-\tfrac{t}{2}\right)\hat{P}_b-\left(R-\tfrac{t}{2}\right)\hat{T}_{b,\varphi}-1-\textstyle\sum_{i=1}^{N}\left[\left(\bar{Q}^{(i)}-\bar{Q}^{(i-1)}\right)\mathbf{h}^T(t_{i-1})\mathbf{s}\mathcal{F}\right.\\ &+ \left(\bar{Q}^{(i)}-\bar{Q}^{(i-1)}\right)\mathbf{m}^T(t_{i-1})\mathbf{s}\mathcal{F}_{,\varphi\varphi}\\ &+ \left.\tfrac{1}{t_{i-1}+R}\left(\bar{Q}^{(i)}-\bar{Q}^{(i-1)}\right)\mathbf{g}^T(t_{i-1})\mathbf{s}\mathcal{F}_{,\varphi\varphi}\right].\end{aligned} \tag{A.5}$$

Hence we find for $\left(R+\frac{t}{2}\right)\sigma_r(z=t/2)$:

$$\begin{aligned}\left(R+\tfrac{t}{2}\right)\sigma_r(t/2) &= \textstyle\sum_{k=1}^{N}\left(\frac{1}{t_k+R}-\frac{1}{t_{k-1}+R}\right)\left(R-\frac{t}{2}\right)^2\hat{T}_{b,\varphi}+\left(R-\tfrac{t}{2}\right)\hat{P}_b\\ &+ \textstyle\sum_{k=1}^{N}\left[\bar{Q}^{(k)}\mathbf{h}^T(t_k)-\bar{Q}^{(k)}\mathbf{h}^T(t_{k-1})\right]\mathbf{s}\mathcal{F}\\ &+ \textstyle\sum_{k=1}^{N}\left[\bar{Q}^{(k)}\mathbf{m}^T(t_k)-\bar{Q}^{(k)}\mathbf{m}^T(t_{k-1})\right]\mathbf{s}\mathcal{F}_{,\varphi\varphi}\\ &+ \textstyle\sum_{k=1}^{N}\left[\frac{1}{t_k+R}\sum_{i=1}^{k}\left[\left(\bar{Q}^{(i)}-\bar{Q}^{(i-1)}\right)\mathbf{g}^T(t_{i-1})\right]\mathbf{s}\mathcal{F}_{,\varphi\varphi}\right.\\ &- \left.\tfrac{1}{t_{k-1}+R}\textstyle\sum_{i=1}^{k-1}\left[\left(\bar{Q}^{(i)}-\bar{Q}^{(i-1)}\right)\mathbf{g}^T(t_{i-1})\right]\mathbf{s}\mathcal{F}_{,\varphi\varphi}\right]\end{aligned} \tag{A.6}$$

which fulfils the equilibrium equation (27) as we know that $\left(R-\frac{t}{2}\right)\sigma_r(-t/2)=\left(R-\frac{t}{2}\right)\hat{P}_b$.

Appendix B. Integration of the equilibrium equations

In the Hellinger-Reissner mixed variational principle of an equivalent single layer, Cauchy's equilibrium conditions are integrated in the thickness direction and then added to the potential energy as constraints via Lagrange multipliers. Hence, we integrate the equilibrium equations (9) and (10) in the r-direction and combine them with equation (6). First, the hoop equilibrium equation (9) is multiplied by $r=z+R$ and then integrated with with respect to $dr=dz$. Noting that $\sigma_{r\varphi,r}=\sigma_{r\varphi,z}$, we get:

$$\int(z+R)\,\sigma_{r\varphi,z}dz+2\int\sigma_{r\varphi}dz+\int\sigma_{\varphi,\varphi}dz=0 \tag{B.1}$$

and using integration by parts on the first term results in:

$$\left(\frac{t}{2}+R\right)\hat{T}_t-\left(-\frac{t}{2}+R\right)\hat{T}_b-\int\sigma_{r\varphi}dz+2\int\sigma_{r\varphi}dz+\int\sigma_{\varphi,\varphi}dz=0. \tag{B.2}$$

Now, using the definition of N_φ and Q_φ in equation (6) to integrate σ_φ and $\sigma_{r\varphi}$ gives:

$$\left(\frac{t}{2}+R\right)\hat{T}_t-\left(-\frac{t}{2}+R\right)\hat{T}_b+Q_\varphi+N_{\varphi,\varphi}=0. \tag{B.3}$$

Next, the hoop equilibrium equation (9) is multiplied by $r=z+R$ and then integrated with respect to $zdr=zdz$, i.e. the balance of moments about the mid-plane is evaluated. Hence:

$$\int z\,(z+R)\,\sigma_{r\varphi,z}dz+2\int z\sigma_{r\varphi}dz+\int z\sigma_{\varphi,\varphi}dz=0 \tag{B.4}$$

and using integration by parts on the first term we get:

$$\begin{aligned}\left[z^2+Rz\right]\Big|^{t/2}\hat{T}_t-\left[z^2+Rz\right]\Big|^{-t/2}\hat{T}_b-\int(2z+R)\,\sigma_{r\varphi}dz\\ +2\int z\sigma_{r\varphi}dz+\int z\sigma_{\varphi,\varphi}dz=0.\end{aligned}\tag{B.5}$$

Now, using the definition of M_φ and Q_φ in equation (6) to integrate σ_φ and $\sigma_{r\varphi}$ gives:

$$\left[\left(\frac{t}{2}\right)^2+R\left(\frac{t}{2}\right)\right]\hat{T}_t-\left[\left(-\frac{t}{2}\right)^2+R\left(-\frac{t}{2}\right)\right]\hat{T}_b-RQ_\varphi+M_{\varphi,\varphi}=0\tag{B.6}$$

such that, by rearranging equation (B.6), we find for Q_φ:

$$Q_\varphi=\frac{1}{R}\left[\left\{\left(\frac{t}{2}\right)^2+R\left(\frac{t}{2}\right)\right\}\hat{T}_t-\left\{\left(-\frac{t}{2}\right)^2+R\left(-\frac{t}{2}\right)\right\}\hat{T}_b+M_{\varphi,\varphi}\right].\tag{B.7}$$

Substituting equation (B.7) into (B.3) we find:

$$\begin{aligned}&\left(\tfrac{t}{2}+R\right)\hat{T}_t-\left(-\tfrac{t}{2}+R\right)\hat{T}_b\\ &\quad+\tfrac{1}{R}\left[\left\{\left(\tfrac{t}{2}\right)^2+R\left(\tfrac{t}{2}\right)\right\}\hat{T}_t-\left\{\left(-\tfrac{t}{2}\right)^2+R\left(-\tfrac{t}{2}\right)\right\}\hat{T}_b+M_{\varphi,\varphi}\right]+N_{\varphi,\varphi}=0\\ &\therefore\left(1+\tfrac{t}{2R}\right)\left(R+\tfrac{t}{2}\right)\hat{T}_t-\left(1-\tfrac{t}{2R}\right)\left(R-\tfrac{t}{2}\right)\hat{T}_b+\tfrac{1}{R}M_{\varphi,\varphi}+N_{\varphi,\varphi}=0.\end{aligned}\tag{B.8}$$

Next, we multiply the radial equilibrium equation (10) by $r=z+R$ and integrate with respect to $dr=dz$. Noting that $\sigma_{r,r}=\sigma_{r,z}$ we get:

$$\int(z+R)\,\sigma_{r,z}dz+\int\sigma_r dz-\int\sigma_\varphi dz+\int\sigma_{r\varphi,\varphi}dz=0.\tag{B.9}$$

Using integration by parts on the first term in equation (B.9) gives:

$$\begin{aligned}\left\{\left(\tfrac{t}{2}\right)+R\right\}\hat{P}_t-\left\{\left(-\tfrac{t}{2}\right)+R\right\}\hat{P}_b-\int\sigma_r dr+\int\sigma_r dr\\ -\int\sigma_\varphi dr+\int\sigma_{r\varphi,\varphi}dr=0.\end{aligned}\tag{B.10}$$

And using the definition of N_φ and Q_φ in equation (6) to integrate σ_φ and $\sigma_{r\varphi}$ results in:

$$\left\{\left(\frac{t}{2}\right)+R\right\}\hat{P}_t-\left\{\left(-\frac{t}{2}\right)+R\right\}\hat{P}_b-N_\varphi+Q_{\varphi,\varphi}=0.\tag{B.11}$$

Substituting equation (B.7) in (B.11) yields:

$$\begin{aligned}&\left\{\left(\tfrac{t}{2}\right)+R\right\}\hat{P}_t-\left\{\left(-\tfrac{t}{2}\right)+R\right\}\hat{P}_b-N_\varphi\\ &\quad+\tfrac{1}{R}\left[\left\{\left(\tfrac{t}{2}\right)^2+R\left(\tfrac{t}{2}\right)\right\}\hat{T}_{t,\varphi}-\left\{\left(-\tfrac{t}{2}\right)^2+R\left(-\tfrac{t}{2}\right)\right\}\hat{T}_{b,\varphi}+M_{\varphi,\varphi\varphi}\right]=0\\ &\therefore\left(\tfrac{t}{2}+R\right)\hat{P}_t-\left(-\tfrac{t}{2}+R\right)\hat{P}_b-N_\varphi\\ &\quad+\tfrac{1}{R}\left[\tfrac{t}{2}\left\{\left(R+\tfrac{t}{2}\right)\hat{T}_{t,\varphi}+\left(R-\tfrac{t}{2}\right)\hat{T}_{b,\varphi}\right\}+M_{\varphi,\varphi\varphi}\right]=0\end{aligned}\tag{B.12}$$

Thus, equations (B.8) and (B.12) represent the classical membrane and bending equilibrium equations written in terms of the classical membrane force N_φ and bending moment M_φ.

Appendix C. Derivation of the potential energy term

The term Π_Γ is:

$$\begin{aligned}
\Pi_\Gamma &= -\int_\Gamma \left(\sigma_\varphi^T \hat{u}_\varphi^{(k)} + \sigma_{r\varphi}\hat{w}_0\right) d\Gamma \\
&= -\int \left(\sigma_\varphi^T \mathbf{f}^T \hat{\mathcal{U}}_\varphi + \sigma_{r\varphi}\hat{w}_0\right)\Big|_{\varphi_A}^{\varphi_B} dz \\
&= -\int \sigma_\varphi^T \mathbf{f}^T \hat{\mathcal{U}}_\varphi\Big|_{\varphi_A}^{\varphi_B} dz - Q_\varphi \hat{w}_0\Big|_{\varphi_A}^{\varphi_B} \\
&= -\int \left(\mathbf{f}\sigma_\varphi\right)^T\Big|_{\varphi_A}^{\varphi_B} dz\hat{\mathcal{U}}_\varphi \\
&- \frac{1}{R}\left[\left\{\left(\frac{t}{2}\right)^2 + R\left(\frac{t}{2}\right)\right\}\hat{T}_t - \left\{\left(-\frac{t}{2}\right)^2 + R\left(-\frac{t}{2}\right)\right\}\hat{T}_b + M_{\varphi,\varphi}\right]\hat{w}_0\Big|_{\varphi_A}^{\varphi_B} \\
&= -\mathcal{F}^T\hat{\mathcal{U}}_\varphi\Big|_{\varphi_A}^{\varphi_B} - \frac{1}{R}\left[\left\{\left(\frac{t}{2}\right)^2 + R\left(\frac{t}{2}\right)\right\}\hat{T}_t\right. \\
&- \left.\left\{\left(-\frac{t}{2}\right)^2 + R\left(-\frac{t}{2}\right)\right\}\hat{T}_b + M_{\varphi,\varphi}\right]\hat{w}_0\Big|_{\varphi_A}^{\varphi_B}
\end{aligned} \tag{C.1}$$

where φ_A and φ_B are the two endpoints of the curved beam, and $\hat{\mathcal{U}}_\varphi = (\hat{u}_0\ \hat{u}_1\ \dots)^T$ are the prescribed mid-plane displacements at φ_A and φ_B. The term Π_λ is:

$$\begin{aligned}
\Pi_\lambda &= \int \lambda_1\left[\left(1+\frac{t}{2R}\right)\left(R+\frac{t}{2}\right)\hat{T}_t - \left(1-\frac{t}{2R}\right)\left(R-\frac{t}{2}\right)\hat{T}_b + \frac{1}{R}M_{\varphi,\varphi} + N_{\varphi,\varphi}\right]d\varphi \\
&+ \int \lambda_2\left[\left(\frac{t}{2}+R\right)\hat{P}_t - \left(-\frac{t}{2}+R\right)\hat{P}_b - N_\varphi\right. \\
&+ \left.\frac{1}{R}\left[\frac{t}{2}\left\{\left(R+\frac{t}{2}\right)\hat{T}_{t,\varphi} + \left(R-\frac{t}{2}\right)\hat{T}_{b,\varphi}\right\} + M_{\varphi,\varphi\varphi}\right]\right]d\varphi
\end{aligned} \tag{C.2}$$

The term Π_φ is:

$$\begin{aligned}
\Pi_\varphi &= \frac{1}{2}\int\int \sigma_\varphi^T \epsilon_\varphi r dr d\varphi \\
&= \frac{1}{2}\int\int \sigma_\varphi^T\left(\frac{1}{r}\mathbf{f}^T\mathbf{s}\mathcal{F}\right) r dr d\varphi \\
&= \frac{1}{2}\int\int\left(\frac{1}{r}\bar{Q}^{(k)}\mathbf{f}^T\mathbf{s}\mathcal{F}\right)^T\mathbf{f}^T\mathbf{s}\mathcal{F}\, dr d\varphi \\
&= \frac{1}{2}\int \mathcal{F}^T\mathbf{s}^T\int\frac{1}{z+R}\mathbf{f}\bar{Q}^{(k)}\mathbf{f}^T dz\mathbf{s}\mathcal{F}\, d\varphi \\
&= \frac{1}{2}\int \mathcal{F}^T\mathbf{s}^T\mathbf{S}\mathbf{s}\mathcal{F}\, d\varphi \\
&= \frac{1}{2}\int \mathcal{F}^T\mathbf{s}^T\mathcal{F}\, d\varphi
\end{aligned} \tag{C.3}$$

The term $\Pi_{r\varphi}$ is:

$$\begin{aligned}
\Pi_{r\varphi} &= \frac{1}{2}\int\int \sigma_{r\varphi}^T \epsilon_{r\varphi} r dr d\varphi \\
&= \frac{1}{2}\int\int \frac{1}{(z+R)^2}\left(\gamma^{(k)}(z)\mathbf{s}\mathcal{F}_{,\varphi} + \left(R-\frac{t}{2}\right)^2\hat{T}_b\right)^T \\
&\quad\cdot\frac{1}{G_{r\varphi}^{(k)}}\frac{1}{(z+R)^2}\left(\gamma^{(k)}(z)\mathbf{s}\mathcal{F}_{,\varphi} + \left(R-\frac{t}{2}\right)^2\hat{T}_b\right)(z+R)\, dz d\varphi \\
&= \frac{1}{2}\int\int \frac{1}{(z+R)^3 G_{r\varphi}^{(k)}}\left(\mathcal{F}_{,\varphi}^T\mathbf{s}^T\left(\gamma^{(k)}\right)^T\gamma^{(k)}\mathbf{s}\mathcal{F}_{,\varphi}\right. \\
&+ \left. 2\mathcal{F}_{,\varphi}^T\mathbf{s}^T\left(\gamma^{(k)}\right)^T\left(R-\frac{t}{2}\right)^2\hat{T}_b + \left(R-\frac{t}{2}\right)^4\hat{T}_b^2\right) dz d\varphi \\
&= \frac{1}{2}\int\left[\mathcal{F}_{,\varphi}^T\eta\mathcal{F}_{,\varphi} + 2\mathcal{F}_{,\varphi}^T\chi\left(R-\frac{t}{2}\right)^2\hat{T}_b\right. \\
&- \left.\frac{1}{2(z+R)^2 G_{r\varphi}^{(k)}}\Big|_{-t/2}^{t/2}\left(R-\frac{t}{2}\right)^4\hat{T}_b^2\right] d\varphi
\end{aligned} \tag{C.4}$$

where $\gamma^k(z)$ is a function of z which we define as:

$$\gamma^{(k)}(z) = -\bar{Q}^{(k)}\mathbf{g}^T + \sum_{i=1}^{k}\left[\left(\bar{Q}^{(i)} - \bar{Q}^{(i-1)}\right)\mathbf{g}^T(t_{i-1})\right] \tag{C.5}$$

and η and χ are shear correction factors defined as:

$$\begin{aligned} \eta &= \int_{-t/2}^{t/2} \frac{1}{(z+R)^3 G_{r\varphi}^{(k)}}\left(\mathbf{s}^T\left(\gamma^{(k)}\right)^T\gamma^{(k)}\mathbf{s}\right)dz \\ \chi &= \int_{-t/2}^{t/2} \frac{1}{(z+R)^3 G_{r\varphi}^{(k)}}\left(\mathbf{s}^T\left(\gamma^{(k)}\right)^T\right)dz \end{aligned} \tag{C.6}$$

Appendix D. First variation of the potential energy

Using equation (C.1), the first variation of $\delta\Pi_\Gamma$ is:

$$\begin{aligned} \delta\Pi_\Gamma &= -\delta\Big[\mathcal{F}^T\hat{\mathcal{U}}_\varphi + \tfrac{1}{R}\Big[\left\{\left(\tfrac{t}{2}\right)^2 + R\left(\tfrac{t}{2}\right)\right\}\hat{T}_t \\ &- \left\{\left(-\tfrac{t}{2}\right)^2 + R\left(-\tfrac{t}{2}\right)\right\}\hat{T}_b + M_{\varphi,\varphi}\Big]\hat{w}_0\Big]_{\varphi_A}^{\varphi_B} \\ &= -\left[\delta\mathcal{F}^T\hat{\mathcal{U}}_\varphi + \tfrac{1}{R}\delta M_{\varphi,\varphi}\hat{w}_0\right]_{\varphi_A}^{\varphi_B} \end{aligned} \tag{D.1}$$

Using equation (C.2), the variation $\delta\Pi_{\lambda_1}$ is:

$$\begin{aligned} \delta\Pi_{\lambda_1} &= \int \delta\lambda_1\Big[\left(1+\tfrac{t}{2R}\right)\left(R+\tfrac{t}{2}\right)\hat{T}_t - \left(1-\tfrac{t}{2R}\right)\left(R-\tfrac{t}{2}\right)\hat{T}_b \\ &+ \tfrac{1}{R}M_{\varphi,\varphi} + N_{\varphi,\varphi}\Big]d\varphi + \int \tfrac{1}{R}\lambda_1\delta M_{\varphi,\varphi}d\varphi + \int \lambda_1\delta N_{\varphi,\varphi}d\varphi \\ &= \int \delta\lambda_1\Big[\left(1+\tfrac{t}{2R}\right)\left(R+\tfrac{t}{2}\right)\hat{T}_t - \left(1-\tfrac{t}{2R}\right)\left(R-\tfrac{t}{2}\right)\hat{T}_b \\ &+ \tfrac{1}{R}M_{\varphi,\varphi} + N_{\varphi,\varphi}\Big]d\varphi + \int -\tfrac{1}{R}\lambda_{1,\varphi}\delta M_\varphi d\varphi \\ &+ \tfrac{1}{R}\lambda_1\delta M_\varphi\Big|_{\varphi_A}^{\varphi_B} + \lambda_1\delta N_\varphi\Big|_{\varphi_A}^{\varphi_B} - \int \lambda_{1,\varphi}\delta N_\varphi d\varphi \end{aligned} \tag{D.2}$$

Using equation (C.2), the variation $\delta\Pi_{\lambda_2}$ is:

$$\begin{aligned} \delta\Pi_{\lambda_2} &= \int \delta\lambda_2\Big[\left(\tfrac{t}{2}+R\right)\hat{P}_t - \left(-\tfrac{t}{2}+R\right)\hat{P}_b - N_\varphi \\ &+ \tfrac{1}{R}\Big[\tfrac{t}{2}\left\{\left(R+\tfrac{t}{2}\right)\hat{T}_{t,\varphi} + \left(R-\tfrac{t}{2}\right)\hat{T}_{b,\varphi}\right\} + M_{\varphi,\varphi\varphi}\Big]\Big]d\varphi \\ &- \int \lambda_2\delta N_\varphi d\varphi + \int \lambda_2\tfrac{1}{R}\delta M_{\varphi,\varphi\varphi}d\varphi \\ &= \int \delta\lambda_2\Big[\left(\tfrac{t}{2}+R\right)\hat{P}_t - \left(-\tfrac{t}{2}+R\right)\hat{P}_b - N_\varphi \\ &+ \tfrac{1}{R}\Big[\tfrac{t}{2}\left\{\left(R+\tfrac{t}{2}\right)\hat{T}_{t,\varphi} + \left(R-\tfrac{t}{2}\right)\hat{T}_{b,\varphi}\right\} + M_{\varphi,\varphi\varphi}\Big]\Big]d\varphi \\ &- \int \lambda_2\delta N_\varphi d\varphi + \tfrac{1}{R}\lambda_2\delta M_{\varphi,\varphi}\Big|_{\varphi_A}^{\varphi_B} - \tfrac{1}{R}\lambda_{2,\varphi}\delta M_\varphi\Big|_{\varphi_A}^{\varphi_B} \\ &+ \int \tfrac{1}{R}\lambda_{2,\varphi\varphi}\delta M_\varphi d\varphi \end{aligned} \tag{D.3}$$

Using equation (C.3), the variation $\delta\Pi_\varphi$ is:

$$\begin{aligned} \delta\Pi_\varphi &= \delta\left[\tfrac{1}{2}\int \mathcal{F}^T\mathbf{s}^T\mathcal{F}d\varphi\right] \\ &= \int \mathcal{F}^T\mathbf{s}^T\delta\mathcal{F}d\varphi \end{aligned} \tag{D.4}$$

Using equation (C.4), the variation $\delta\Pi_{r\varphi}$ is:

$$\begin{aligned} \delta\Pi_{r\varphi} &= \int \mathcal{F}_{,\varphi}^T\eta\delta\mathcal{F}_{,\varphi} + \delta\mathcal{F}_{,\varphi}^T\chi\left(R-\tfrac{t}{2}\right)^2\hat{T}_b d\varphi \\ &= \mathcal{F}_{,\varphi}^T\eta\delta\mathcal{F}\Big|_{\varphi_A}^{\varphi_B} + \delta\mathcal{F}^T\chi\left(R-\tfrac{t}{2}\right)^2\hat{T}_b\Big|_{\varphi_A}^{\varphi_B} - \int \mathcal{F}_{,\varphi\varphi}^T\eta\delta\mathcal{F}d\varphi \\ &- \int \delta\mathcal{F}^T\chi\left(R-\tfrac{t}{2}\right)^2\hat{T}_{b,\varphi}d\varphi. \end{aligned} \tag{D.5}$$

Appendix E. Calculation of the stress residual

The derivatives needed to calculate the stress residuals can be expressed as follows:

$$
\begin{aligned}
\sigma_{\varphi,\varphi} &= \bar{Q}^{(k)} \tfrac{1}{r} \mathbf{f}^T \mathbf{s}\mathcal{F}_{,\varphi} \\
\sigma_{r\varphi,\varphi} &= \tfrac{1}{r^2} \left(-\bar{Q}^{(k)} \mathbf{g}^T \mathbf{s}\mathcal{F}_{,\varphi\varphi} \right. \\
&+ \left. \textstyle\sum_{i=1}^{k} \left[\left(\bar{Q}^{(i)} - \bar{Q}^{(i-1)} \right) \mathbf{g}^T(t_{i-1}) \right] \mathbf{s}\mathcal{F}_{,\varphi\varphi} + \left(-\tfrac{t}{2} + R \right)^2 \hat{T}_{b,\varphi} \right) \\
\sigma_{r\varphi,r} &= -\tfrac{2}{r^3} - \left(-\tfrac{2}{r^3} \mathbf{g}^T + \tfrac{1}{r^2} \mathbf{f}^T \right) \bar{Q}^{(k)} \mathbf{s}\mathcal{F}_{,\varphi} + \left(-\tfrac{2}{r^3} a^{(k)} \right) \\
\sigma_{r,r} &= -\tfrac{1}{r^2} + \left(-\tfrac{1}{r^2} \mathbf{h}^T + \tfrac{1}{r^2} \mathbf{f}^T \right) \bar{Q}^{(k)} \mathbf{s}\mathcal{F} + \left(-\tfrac{1}{r^2} \mathbf{m}^T + \tfrac{1}{r^3} \mathbf{g}^T \right) \bar{Q}^{(k)} \mathbf{s}\mathcal{F}_{,\varphi\varphi} \\
&- \tfrac{2}{r^3} \textstyle\sum_{i=1}^{k} \left[\left(\bar{Q}^{(i)} - \bar{Q}^{(i-1)} \right) \mathbf{g}^T(t_{i-1}) \right] \bar{Q}^{(k)} \mathbf{s}\mathcal{F}_{,\varphi\varphi} \\
&- \tfrac{2}{r^3} \left(R - \tfrac{t}{2} \right)^2 \hat{T}_{b,\varphi} - \tfrac{1}{r^2} b^{(k)}.
\end{aligned}
\tag{E.1}
$$